Mechanisms of Cation Permeation in Cardiac Sodium Channel: Description by Dynamic Pore Model

Yasutaka Kurata,* Ryoichi Sato,# Ichiro Hisatome,§ and Sunao Imanishi*

*Department of Physiology, Kanazawa Medical University, Ishikawa 920-0293, Japan, #Department of Molecular Pharmacology and Biological Chemistry, Northwestern University Medical School, Chicago, Illinois 60611, and §First Department of Internal Medicine, Tottori University School of Medicine, Yonago 683-0826, Japan.

ABSTRACT The selective permeability to monovalent metal cations, as well as the relationship between cation permeation and gating kinetics, was investigated for native tetrodotoxin-insensitive Na-channels in guinea pig ventricular myocytes using the whole-cell patch clamp technique. By the measurement of inward unidirectional currents and biionic reversal potentials, we demonstrate that the cardiac Na-channel is substantially permeable to all of the group Ia and IIIa cations tested, with the selectivity sequence $Na^+ \geq Li^+ > Tl^+ > K^+ > Rb^+ > Cs^+$. Current kinetics was little affected by the permeant cation species and concentrations tested (≤160 mM), suggesting that the permeation process is independent of the gating process in the Na-channel. The permeability ratios determined from biionic reversal potentials were concentration and orientation dependent: the selectivity to Na^+ increased with increasing internal [K^+] or external [Tl^+]. The dynamic pore model describing the conformational transition of the Na-channel pore between different selectivity states could account for all the experimental data, whereas conventional static pore models failed to fit the concentration-dependent permeability ratio data. We conclude that the dynamic pore mechanism, independent of the gating machinery, may play an important physiological role in regulating the selective permeability of native Na-channels.

INTRODUCTION

Cardiac tetrodotoxin (TTX)-insensitive Na-channels are structurally and pharmacologically distinct from TTX-sensitive ones in neurons or skeletal muscles (Doyle et al., 1993; Favre et al., 1995), and so are possibly different in permeability properties as well. There are many reports on the permeability of Na-channels to monovalent metal cations with little fundamental disagreement in the selectivity (Chandler and Meves, 1965; Hille, 1972, 1975; Cahalan and Begenisich, 1976; Ebert and Goldman, 1976; Begenisich and Cahalan, 1980a). However, most of the previous studies were not for cardiac TTX-insensitive but for TTX-sensitive isoforms; thus we have little information on the selective permeability of cardiac Na-channels. In the present study, therefore, we first investigated the permeability and selectivity of cardiac Na-channels to group Ia and IIIa cations. The inward unidirectional current (IUC), defined as the influx of external cations in the absence of internal permeant cations, as well as the biionic reversal potential (V_{rev}) from which the permeability ratio (P_X/P_{Na}) could be determined using the Goldman–Hodgkin–Katz (GHK) equation, was measured for Na-channels in guinea pig ventricular myocytes.

Single-channel analysis of the cation permeation in native (normally inactivating) Na-channels is technically difficult because of the very brief openings. For that reason, all the recent single-channel studies were not for native Na-channels, but for toxin-modified ones. However, the treatment with toxins such as batrachotoxin (BTX) has been shown to change the conductivity and selectivity of Na-channels (Huang et al., 1979; Khodorov, 1985), indicating that a study using the toxins to slow Na-channel inactivation may miss fundamental properties of the cation transfer in native (toxin-unmodified) Na-channels. Accordingly, we explored the selective permeability of native Na-channels in single heart cells, using the whole-cell current recording.

We also examined whether cation permeation could affect gating behavior by analyzing the activation and inactivation kinetics of IUCs recorded for various cation species and concentrations. It was reported for the neuronal TTX-sensitive Na-channel that the voltage dependence of current activation kinetics shifted to the positive potential by 8–10 mV on replacing Na^+ with K^+ in the external solution (Hille, 1972). This finding indicates that the rate of Na-channel activation depends on permeant cation species, and so the cation permeation possibly interacts with the gating machinery (also see Yamamoto et al., 1985; French et al., 1996). As suggested by Eisenman and Horn (1983), occupancy of channel pores by permeating cations may, in general, affect gating mechanisms (also see Chesnoy-Marchais, 1985; Matteson and Swenson, 1986; Shuba et al., 1991; Neyton and Pelleschi, 1991; Demo and Yellen, 1992; Gómez-Lagunas and Armstrong, 1994; Kiss and Korn, 1998). Thus, exploring effects of cation permeation on gating behavior may help us to understand more profoundly essential mechanisms of the selective ion permeation in Na-channels.

In this study, we further developed a novel kinetic "dynamic pore" model, which satisfactorily accounts for all the

Received for publication 13 July 1998 and in final form 24 June 1999.

Address reprint requests to Sunao Imanishi, Department of Physiology, Kanazawa Medical University, 1-1 Daigaku, Uchinada-machi, Kahoku-gun, Ishikawa 920-0293, Japan. Tel.: +81-76-286-2211; Fax: +81-76-286-8010; E-mail: physiol2@kanazawa-med.ac.jp.

0006-3495/99/10/1885/20 $2.00

experimental data, including the concentration-dependent biionic P_X/P_{Na} and the IUC-concentration relation. Biionic P_X/P_{Na} for Na-channels has been reported to depend on concentrations of internal K^+, and other internal and external cations (Cahalan and Begenisich, 1976; Ebert and Goldman, 1976; Begenisich and Cahalan, 1980a; Yamamoto et al., 1985); thus the Na-channel selectivity may vary in response to changes in ionic composition. In the previous studies, the concentration-dependent selectivity was interpreted as reflecting the asymmetric energy profile and multiple occupancy of the static pore (Begenisich and Cahalan, 1980a; Eisenman and Horn, 1983; Pérez-Cornejo and Begenisich, 1994; Wells and Tanaka, 1997). Recently, however, the fluctuating-barrier and the conformational models, which allow structural transitions of channel pores between multiple conformations with different conductivity and selectivity properties, have been proposed for describing permeability properties of several ionic channels other than the Na-channel (Heinemann and Sigworth, 1990, 1991; Lux et al., 1990; Draber et al., 1991; Mironov, 1992; Hainsworth et al., 1994). These dynamic mechanisms may also account for the concentration-dependent changes in the Na-channel selectivity. This paper would be the first report to provide a quantitative basis for the hypothesis that Na-channel pores undergo the permeating cation (occupancy)-regulated transitions between two conformations with different selectivity properties.

MATERIALS AND METHODS

Cell preparation

Single ventricular myocytes were isolated by the enzymatic dissociation technique described by Mitra and Morad (1985). Briefly, hearts were excised from guinea pigs (300–600 g) under pentobarbital anesthesia (30–50 mg/kg, i.p.). Then, the coronary perfusion via the Langendorff apparatus was initiated with Tyrode's solution of the following composition (mM): NaCl, 140; KCl, 5.4; NaH_2PO_4, 0.33; $MgCl_2$, 0.5; $CaCl_2$, 1.8; D-glucose, 5.0; HEPES, 5.0 (pH = 7.4 with NaOH). After 5–10-min perfusion of the nominally Ca^{2+}-free solution, the enzyme solution containing 50–100 units/ml collagenase (Yakult, Tokyo, Japan) was perfused for 10 min. The mechanically dispersed cells were stored in KB medium at 4°C, and studied within 8 hr. KB medium contained (mM) K-glutamate, 70; taurine, 20; KCl, 20; KH_2PO_4, 10; D-glucose, 10; HEPES, 10; EGTA, 0.5 (pH = 7.3 with KOH).

Electrophysiological recording

The whole cell configuration of the patch clamp technique was used for recording Na-channel currents. Pipette electrodes were made from 1.5 mm (o.d.) hematocrit glass capillary tubes with a vertical pipette puller (Narishige PP-83, Tokyo, Japan), having the resistance of 300–500 kΩ when filled with the internal solutions. Liquid junction potentials of the bath (external) solutions to the pipette (internal) solutions were +5 ± 3 mV.

Cell capacitance and series resistance calculated during the capacitive current cancellation ranged 60–180 pF and 0.6–1.5 MΩ, respectively. The series resistance was compensated by 50–70% of the originals. After the compensation, the voltage errors arising from the series resistance (200–800 kΩ) were less than 2 mV; and capacitive transients were completed within 500 μs. Under our experimental conditions, recordings of Na-channel currents satisfied the criteria described by Colatsky and Tsien (1979), which permit the indirect determination of adequacy of space-clamp control.

The membrane potential was held at −80 mV, and depolarizing test pulses were preceded by 1.5–2.0-s hyperpolarization to −140 (or −150) mV for Na-channels to attain full recovery from inactivation. Cells were depolarized once each 2.0–2.5 s (at 0.4–0.5 Hz) for 10–80 ms. Currents were capacity- and leak-corrected by subtracting the currents in response to the test pulses after 1.5–2.0-s conditioning at −60 mV, where the steady-state availability of Na-channels was nearly zero. All experiments were performed at 8–10°C.

Currents were recorded with an EPC-9 amplifier (HEKA electronic, Lambrecht, Germany), and directly stored in a Macintosh Quadra 840AV computer (Apple Computer, Inc., Cupertino, CA) at 10 kHz. The capacity- and leak-corrected data were digitally filtered at 2 kHz, then analyzed with Pulse/Pulsefit (HEKA electronic) and IGOR (Wave Metrics Inc., Lake Oswego, OR) on the Macintosh computer. The curve fitting with the equations described later was performed using a nonlinear least-square algorithm available in the Pulse/Pulsefit program.

Solutions

Measurement of inward unidirectional currents

The composition of internal and external solutions used for the measurement of IUCs is shown in Table 1. To record IUCs, we used the internal

TABLE 1 Composition of solutions for recording inward unidirectional currents

	External Solutions (mM)					
	Test Cation	AC*	TMA	Ca	Anion	HEPES
TMA-sol	–		160 −	2	Cl 164	10
Na-sol	Na 2.5 ~ 10	(0.72)	160 − [Na]	2	Cl 164	10
Li-sol	Li 2.5 ~ 10	(0.77)	160 − [Li]	2	Cl 164	10
KCl-sol	K 20 ~ 160	(0.71)	160 − [K]	2	Cl 164	10
KNO_3-sol	K 20 ~ 160	(0.71)	160 − [K]	2	NO_3 164	10
Rb-sol	Rb 40 ~ 160	(0.70)	160 − [Rb]	2	Cl 164	10
Cs-sol	Cs 40 ~ 160	(0.70)	160 − [Cs]	2	Cl 164	10
Tl-sol	Tl 5 ~ 160	(0.70)	160 − [Tl]	2	NO_3 164	10

	Internal Solutions (mM)				
	Test Cation	TMA	Cl	F	HEPES
TMA-sol	(−)	160	10	150	10

*AC, activity coefficients for the test cations predicted by the Debye–Hückel theory.

(pipette) solution containing an impermeant cation, tetramethylammonium (TMA), as the only monovalent cation. The concentrations of Na^+ and Li^+ were limited to 10 mM, because the large currents yielded by Na^+ or Li^+ at ≥20 mM did not allow satisfactory voltage control. Ionic strength of the test solutions was held constant by adding TMA-salts to the total monovalent cation concentration of 160 mM. Because of the water insolubility of thallium halides, all the components used for Tl-solution (sol) (and for KNO_3-sol) are nitrate salts (see Hille, 1972).

Measurement of biionic reversal potentials

The external and internal solutions used for the biionic V_{rev} measurement are listed in Table 2. The internal concentration of Tl^+ was limited to 10 mM for stable V_{rev} measurement. For blocking the passage of K^+ or Tl^+ through K-channels and minimizing accumulation of these cations at the intracellular space, 10 mM Cs^+ was added to the external K- and Tl-sols. Adding 10 mM Cs^+ to the external Na-sol produced no significant change in V_{rev}.

Activity coefficients for monovalent metal cations

Thermodynamic activities (not concentrations) of the test cations in solution should be used to determine the biionic P_X/P_{Na} from the GHK equation, and to compute the amplitude of currents carried in model pores. According to the Debye–Hückel theory, the activity coefficients for Li^+, Na^+, K^+, Rb^+, Cs^+, and Tl^+ in 0.16 M salt solutions were assumed to be 0.77, 0.72, 0.71, 0.70, 0.70, and 0.70, respectively. The activity coefficient for Tl^+ was set equal to 0.55, because $TlNO_3$ was estimated to be only 78% dissociated in the test solutions (see Hille, 1972).

Experimental procedures

Measurement of inward unidirectional currents

Cells were internally perfused with the TMA-sol containing no permeant cations, and then exposed to a series of the external test solutions with different permeant cation species or different concentrations of a given cation species. The perfusion of the cell interior with the internal TMA-sol was determined to be complete when time-dependent outward currents were almost entirely abolished in the external TMA-sol. For precluding contamination by previously administered cations, the TMA-sol was perfused until inward currents almost completely disappeared before the subsequent test perfusion. In the experiments with various concentrations of a test cation species, external solutions were perfused in the order of increasing concentration, and then the solution of the lowest concentration was readministered to check the reproducibility. Because time-dependent currents could be quickly and almost completely abolished by perfusing the external TMA-sol during repeated applications of the test cations, multiple concentrations and multiple cation species could be studied in the same cell.

With the TMA-sol inside, time-independent leakage and residual K-channel currents were usually very small. When the linear leak resistance between −100 and 0 mV was less than 500 MΩ, the data were discarded. In some experiments, 50 μM TTX was added to provide evidence that time-dependent currents recorded in a test solution were carried in the Na-channel.

Measurement of biionic reversal potentials

Under biionic conditions with one reference species inside and the other test species outside, currents were recorded during 10–20-ms step depolarizations at 5-mV intervals. A value of V_{rev} was determined for each current family by interpolating peak currents to the zero current axis of the current–voltage (I–V) plot. The reference (control) V_{rev} was also determined with the reference cation at symmetrical concentrations on both sides of the membrane. When the difference between the reference V_{rev} values measured before the first and after the final test recording was >2.0 mV, the data were discarded.

Analysis of selective permeability

Current–concentration relationship

Concentration dependence of the peak amplitude of IUCs was approximated with a Michaelis–Menten equation,

$$I = I_{max}/[1 + (K_m/C)], \quad (1)$$

where I represents the amplitude of peak currents at a concentration of C. I_{max} and K_m are the maximum current and the apparent dissociation constant, respectively.

Biionic permeability ratio

Selectivity to the monovalent metal cations was quantified as the permeability ratio P_X/P_{Na}, which was determined from biionic V_{rev} using the GHK equation. The permeability ratio P_B/P_A is given by a biionic form of the GHK equation,

$$P_B/P_A = ([A^+]_o/[B^+]_o) \cdot \exp(\Delta V_{rev} \cdot F/RT), \quad (2)$$

TABLE 2 Composition of solutions for measurement of biionic reversal potentials

	External Solutions (mM)					
	Test Cation	Cs*	TMA	Ca	Anion	HEPES
Na-sol	Na 2.5 ~ 40		160 − [Na]	2	Cl 164	10
Li-sol	Li 5		155	2	Cl 164	10
K-sol	K 20 ~ 160	10	160 − [K]	2	Cl 164	10
Rb-sol	Rb 160		–	2	Cl 164	10
Cs-sol	Cs 160		–	2	Cl 164	10
Tl-sol	Tl 5 ~ 80	10	160 − [Tl]	2	NO_3 164	10

	Internal Solutions (mM)				
	Test Cation	TMA	Cl	F	HEPES
Na-sol	Na 5 ~ 10	160 − [Na]	10	150	10
K-sol	K 40 ~ 160	160 − [K]	10	150	10
Tl-sol	Tl 10	150	5	155	10

*For blocking K-channel currents, 10 mM Cs^+ was added to the external K- and Tl-sols.

where ΔV_{rev} represents the change in V_{rev} on replacing the reference cation A^+ with the test cation B^+ in the bath. The constants F, R, and T have their conventional thermodynamic meanings ($F/RT = 0.041\ mV^{-1}$ at 10°C).

Analysis of gating kinetics

Steady-state availability

Voltage-dependent steady-state availability was fitted by a Boltzmann distribution,

$$I/I_{max} = 1/[1 + \exp\{(V_C - V_H)/s\}]. \quad (3)$$

Here, the peak current (I) in the test depolarization to −20 mV after conditioning at various voltages (V_C) is expressed relative to the maximum peak current (I_{max}). Parameters estimated by the fit were the voltage of the half-point (V_H) and the slope factor (s), both expressed in mV.

Activation kinetics (time to peak current)

To quantify the shift in voltage dependence of the time to peak current (T_P), we used the equation,

$$T_P(V_t) = T_C + T_I \cdot \exp\{-S \cdot (V_t + 40)\}. \quad (4)$$

Following Hanck and Sheets (1992b), we constrained T_C and S to the values required to fit the control data (for Na^+). Then, a shift of the T_P–voltage relation for cation X^+ relative to that for Na^+ (ΔV_P) is given by

$$\Delta V_P = -(1/S) \cdot \ln(T_{INa}/T_{IX}), \quad (5)$$

where the T_I values for Na^+ and X^+ are denoted T_{INa} and T_{IX}, respectively.

Inactivation kinetics

The decay phase of Na-channel currents over the voltage range from −60 to +20 mV was fitted by a double exponential function,

$$I(t) = a_F \cdot \exp(-t/\tau_F) + a_S \cdot \exp(-t/\tau_S), \quad (6)$$

where $I(t)$ represents the amplitude of currents at time t, with τ being the time constant of fast (τ_F) or slow (τ_S) inactivation. The initial values extrapolated to time zero for the fast and slow components are denoted a_F and a_S, respectively. According to Hanck and Sheets (1992b), the τ_F–voltage relation was fitted to an exponential function,

$$\tau_F(V_t) = \tau_C + \tau_I \cdot \exp\{-S \cdot (V_t + 40)\}. \quad (7)$$

A shift of the τ_F–voltage relation for cation X^+ relative to that for Na^+ (ΔV_I) is given by

$$\Delta V_I = -(1/S) \cdot \ln(\tau_{INa}/\tau_{IX}), \quad (8)$$

where τ_{INa} and τ_{IX} represent the τ_I values for Na^+ and X^+, respectively.

Vestibule surface potential and surface charge effects

Na-channels are known to carry fixed negative charges arising from an excess of acidic amino acid residues located in the channel vestibules (Green et al., 1987; Cai and Jordan, 1990). These permanent charges, creating the vestibule surface potential (V_S), would affect cation permeation, selectivity, and gating kinetics (Dani, 1986; Cai and Jordan, 1990; Dani and Fox, 1991; Correa et al., 1991; Hanck and Sheets, 1992b; Naranjo and Latorre, 1993). Therefore, we considered the effects of V_S and the charge screening or binding by permeant cations in analyzing the Na-channel permeability as well as the gating property.

We approximated V_S according to the Gouy–Chapman–Stern (GCS) double layer theory (see Dani, 1986; Hanck and Sheets, 1992b; Naranjo and Latorre, 1993). The relation of V_S (mV) to the density of cation-free surface charge sites to be screened (denoted σ_F in sites/nm^2) is described by the Grahame equation,

$$\sigma_F = (1/G)[C_1 \cdot \exp(-V_S F/RT) - C_1 + C_2 \cdot \exp(-2V_S F/RT) - C_2]^{1/2}, \quad (9)$$

where the bulk concentrations of monovalent and divalent cations are denoted C_1 and C_2 (both in M), respectively. The constant G can be set equal to 2.71 at 10°C.

In addition to the screening effect, some cations also reduce V_S by binding to the surface charges. According to Hanck and Sheets (1992b), σ_F can be expressed as

$$\sigma_F = \sigma_T/(1 + \sum[C_i \cdot \exp(-V_S z_i F/RT)/K_{Di}]), \quad (10)$$

where σ_T is the total density of surface charge sites, being set equal to 0.72 sites/nm^2. The dissociation constant for binding the ith cation species is denoted K_{Di} (in M), with C_i being the bulk concentration (in M) and z_i the valency. We calculated V_S by simultaneously solving Eqs. 9 and 10 with the preselected K_D values (0.05 M through infinity for the monovalent metal cations, and 1.2 M for Ca^{2+}).

Kinetic modeling of cation permeation

We examined how well the permeability properties of the Na-channel observed in this study (e.g., *I–V* and IUC–concentration relations, biionic P_X/P_{Na}) can be described by the two types of model pore: 1) static pore of a rigid structure, and 2) "dynamic pore," which undergoes the cation-regulated transition between two conformations with different selectivity properties. State diagrams and mathematical procedures for the dynamic pore model are shown in the Results and in the Appendix; those for the static pore model are essentially the same as described previously (Hille and Schwarz, 1978; Begenisich and Cahalan, 1980a).

Kinetics of ion translocation in the channel pore was described by the discrete energy barrier models based on the Eyring absolute reaction rate theory. We used the two-barrier single-site (2B1S), three-barrier two-site (3B2S) single-occupancy, and 3B2S double-occupancy models. For simplicity, the dynamic pore was assumed to have the 2B1S energy profile, whereas all the energy models were tested for the static pore. (General Gibbs free energy profiles for the 2B1S and 3B2S models are depicted in Fig. A1 in the Appendix.) Rate constants of ion translocation were calculated from the rate theory formulas expressed as functions of total free energies at peaks, wells, and vestibules. Mathematical expressions for the total free energies and transition rate constants are given in the Appendix.

The pore models actually have far more free parameters than can be determined from the experiments, so that it is not possible to optimize all the model parameters. Therefore, the electrical distances in the energy profiles for ion translocation were preselected and held constant while adjusting the parameters (see the Appendix). The first step of the fitting procedure was to systematically compute *I–V* and IUC–concentration curves from the models, thereby searching a set of the parameters (e.g., energy peak heights, well depths, rate constants of conformational transitions) to give satisfactory fit for the experimental observations. The most promising set of the parameters was then selected and refined for each model to fit the biionic P_X/P_{Na} data. The theoretical P_X/P_{Na}, as defined by Eq. 2, was determined from the V_{rev} in *I–V* relation predicted by the models.

Programming for mathematical analyses and numeric calculations with matrix equations were performed on a Power Macintosh 7600/200 computer (Apple Computer, Inc., Cupertino, CA) using MATLAB, a numeric computation and visualization software for the sciences, from MathWorks, Inc. (Natick, MA).

RESULTS

Inward unidirectional currents carried by monovalent metal cations

Figure 1 shows an example of the families of IUCs recorded from a guinea pig ventricular cell bathed in the external solutions containing either TMA alone, one of the group Ia cations (Li^+, Na^+, K^+, Rb^+, Cs^+), or the group IIIa cation Tl^+ (see Table 1). Voltage- and time-dependent IUCs were measurable for all the monovalent metal cations tested. The current families were very similar in the kinetics of current activation and inactivation, and all the time-dependent currents were completely abolished by 50 μM TTX. The currents evoked in the external TMA-sol were very small (<1 pA/pF) but clearly appreciable as compared with the records after TTX perfusion, being possibly carried by Ca^{2+}. According to the previous report by Hille (1972), Tl^+ was so toxic to the nerve membrane that the perfusion of Tl^+ solutions caused the rundown of Na^+ currents as well as the very low membrane resistance. In this study, however, most of the cells tested were tolerant of Tl^+: the Na^+ currents recorded before and after the exposure to Tl-sols were nearly identical.

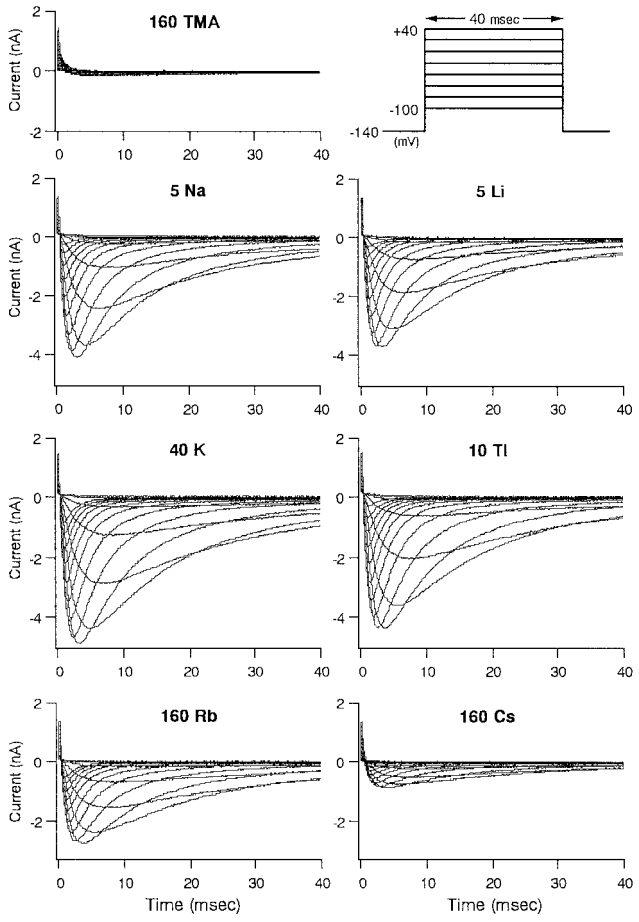

FIGURE 1 Families of IUCs carried by the monovalent metal cations during 40-msec step depolarizations to the test potentials ranging from −100 to +40 mV in 10-mV increments. All currents were recorded in the same cell. The order of perfusion of the external test solutions was TMA-, Cs-, Rb-, KCl-, Li-, Na-, KNO_3-, Tl-sol (currents in KNO_3-sol were not shown). TMA-sol was perfused for 5 min before each application of the test solutions containing the metal cations. The numbers above the current families represent the extracellular cation concentrations in mM.

Influence of cation permeation on gating kinetics

Gating kinetics does not depend on permeant cation species

Figure 2 shows the effects of permeant cation species on the kinetics of Na-channel currents such as the peak IUC–voltage relation, steady-state availability, time to peak current (T_P), and fast inactivation (τ_F). The availability curve (half-point V_H), as well as the peak IUC–voltage relation, shifted toward the negative potentials in accordance with the order of perfusion of all the test solutions except Tl-sol in which the small depolarizing shifts occurred. Coincident with the shifts in the availability and *I–V* curves, there were significant changes in both T_P– and τ_F–voltage relation, which were parallel to those in the availability curve (Fig. 2 *F*). This finding indicates that all the voltage shifts in the kinetic parameters are chiefly due to the time-dependent spontaneous negative shift (see Kimitsuki et al., 1990; Hanck and Sheets, 1992a) or surface charge effects. The rates of the hyperpolarizing shifts during a series of recordings were <10 mV/h, being less than those reported for canine Purkinje cells (>20 mV/h, Hanck and Sheets, 1992a).

Thallous ion apparently affects gating kinetics via surface charge binding effect

Voltage-dependent kinetics of K^+ and Tl^+ currents was further determined at various concentrations. As shown in Fig. 3, *A–D*, the increase in external [Tl^+] led to the positive shift in the availability curve as well as in the peak *I–V* relation, whereas the voltage dependence of K^+ current kinetics little changed with increasing external [K^+]. When Tl-sols containing 5–100 mM Tl^+ were consecutively perfused over the same cell, the V_H of availability curves positively shifted with the linear concentration dependence (Fig. 3 *E*). Assuming that the voltage shifts in availability curves entirely reflect the changes in V_S, the K_D value for Tl^+ binding to a negative surface charge was approximated to be 6.0 M from the GCS analysis, being fivefold higher than that reported for Ca^{2+} (1.2 M, Hanck and Sheets, 1992b). Similarly, both T_P– and τ_F–voltage curves shifted toward the depolarizing direction as external [Tl^+] was raised; the shifts were parallel to those in the availability curve (Fig. 3 *F*).

Selective permeability to monovalent metal cations

Concentration dependence of inward unidirectional currents

Figure 4 shows the concentration dependence of peak IUCs carried by the test cations at −20 mV. Within the concen-

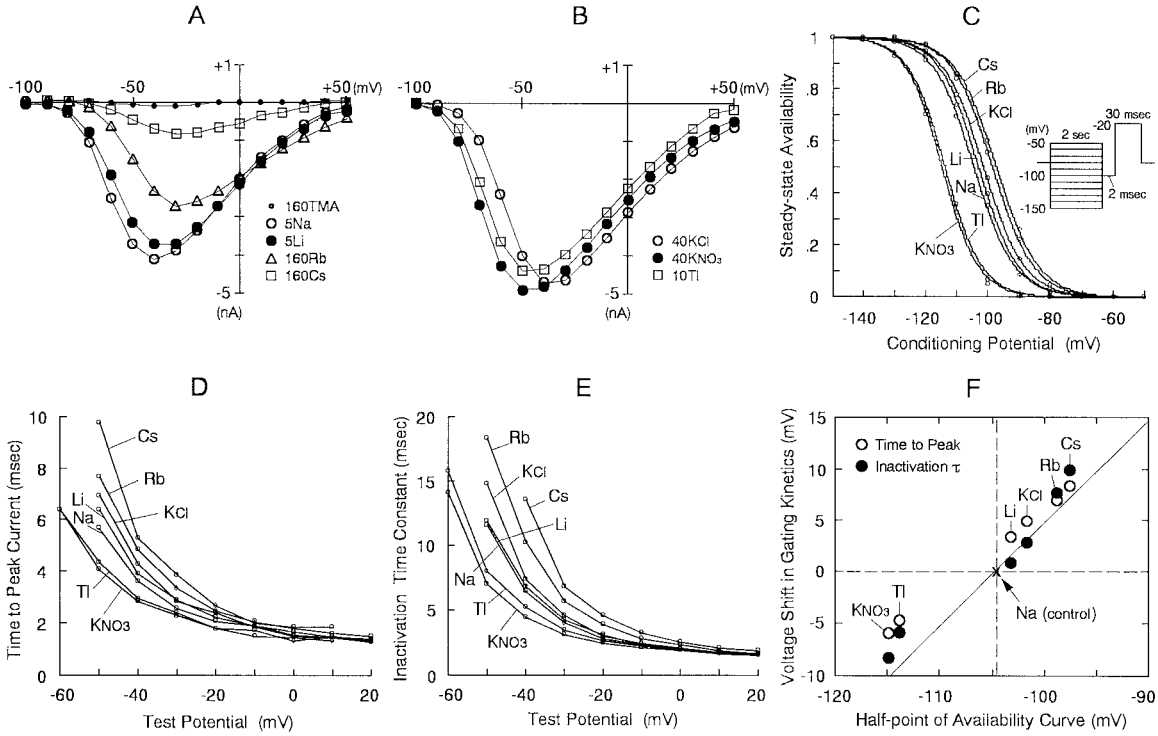

FIGURE 2 Voltage-dependent kinetics of the currents carried by the test cations. (*A*, *B*) Peak IUC-voltage relationships. Currents in response to step depolarizations from a holding potential of −140 (or −150) mV were recorded, and the peak amplitude of capacity-corrected currents was measured after subtractions of time-independent leak currents. (*C*) Steady-state availability curves. As shown in the inset, currents were evoked by the step depolarization to −20 mV after 2-s conditioning pulses ranging from −150 to −50 mV in 10-mV increments. Peak currents were normalized to the maximal current at −150 (or −140) mV, then graphed as a function of the conditioning potentials. The solid lines are the best fits with Eq. 3. (*D*, *E*) Voltage dependence of T_P (*D*) and τ_F (*E*) determined for the identical current records from the same cell as for (*C*). (*F*) Relationships between the voltage shifts in the kinetic parameters. The shift (ΔV) of the T_P- or τ_F-voltage relation for each test cation relative to that for Na^+ was plotted against the half-point (V_H) of the availability curve. Means of the data sets from three cells are shown. The solid line represents a parallel shift in two parameters. The order of perfusion of the test solutions is the same as that in Fig. 1. Changing the external anion from Cl^- to NO_3^- yielded the hyperpolarizing shifts of about 10 mV in the kinetic parameters.

tration range tested (≤160 mM), the peak IUC–concentration relation followed a simple Michaelis–Menten formalism (Eq. 1). As listed in Table 3, the best-fit K_m values for K^+, Rb^+, Cs^+, and Tl^+ were close to those reported for the TTX-sensitive isoform (Hille, 1975). For estimating the relative permeability to the test cations, the IUC ratio, defined as the amplitude of peak IUCs relative to the Na^+ current at the same concentration of *C* mM (abbreviated by $[I_X/I_{Na}]_C$), was determined for each test cation at a low concentration of 5 mM (Present study 1 in Table 3). Thallous ion exhibited the apparently high affinity (K_m = 21.8 mM) and high conductivity at low concentrations ($[I_{Tl}/I_{Na}]_5$ = 0.82) for the cardiac TTX-insensitive Na-channel.

Determination of biionic reversal potential and permeability ratio

The selective permeability to the monovalent metal cations was also examined by a conventional method, that is, the biionic V_{rev} measurement (Fig. 5). The values of V_{rev} measured under various biionic conditions and P_X/P_{Na} computed using Eq. 2 are shown in Fig. 6, as well as in Table 3 with the previously reported data for comparison. The permeability ratios determined by the two distinct methods (i.e., $[I_X/I_{Na}]_5$ from IUC data and P_X/P_{Na} from biionic V_{rev} data) for each test cation were very close, consistent with the notion that biionic P_X/P_{Na} is directly comparable to the conductance ratio in the limit of low ionic concentrations (i.e., at low occupancy of binding-sites) where the conductance is proportional to the permeant ion concentration (Eisenman and Horn, 1983). The selectivity sequence for group Ia cations was $Na^+ \geq Li^+ > K^+ > Rb^+ > Cs^+$ (Eisenman sequence X), being qualitatively the same as for TTX-sensitive isoforms. As shown in Table 3, the relative permeability to K^+, Rb^+, and Tl^+ of the native cardiac Na-channel was greater than that of the native TTX-sensitive one (Hille, 1972), but less than that of the BTX-modified one (Huang et al., 1979).

Dependence of biionic permeability ratio on ionic composition

According to the GHK equation (Eq. 2), the concentration-independent biionic P_X/P_{Na} requires the identical V_{rev} for a constant $[X^+]/[Na^+]$. However, Fig. 5 clearly shows that the V_{rev} values measured with a fixed ratio of internal $[K^+]$ and

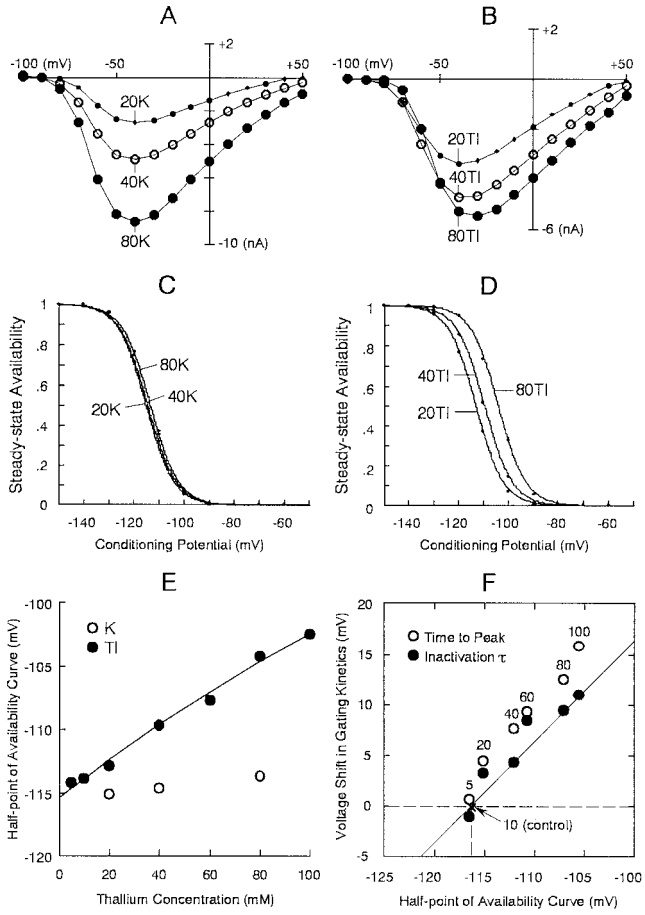

FIGURE 3 Voltage-dependent kinetics of K^+ and Tl^+ currents at various concentrations. (*A*, *B*) Peak IUC-voltage and (*C*, *D*) steady-state availability curves for K^+ (*left*) and Tl^+ (*right*) at 20–80 mM. Cells were consecutively perfused with 20, 40, and 80 mM KNO_3-sols, then with 20, 40, and 80 mM Tl-sols. (*E*) Half-points of steady-state availability curves determined for Tl^+ at 5–100 mM (*closed circles*) and for K^+ at 20–80 mM (*open circles*). The data for Tl^+ and K^+ were obtained from different cells. The solid line is a theoretical prediction of V_H for Tl^+ currents. The changes in the external V_S were calculated by the GCS analysis, and added to the control V_H value at 10 mM. Thallous ion was estimated to have the surface charge binding effect with $K_D = 6.0$ M. (*F*) Relationships between the voltage shifts in Tl^+ current kinetics. The shift (ΔV) of the T_P- or τ_F-voltage relation was plotted against the V_H of the availability curve. The means of three determinations are plotted. The solid line represents a parallel shift in two parameters. Pulse protocols and procedures for data analyses are the same as those for Fig. 2.

external $[Na^+]$ are not the same; therefore, biionic P_K/P_{Na} is concentration dependent. The concentration dependence of P_X/P_{Na} became more manifest when V_{rev} was measured for various biionic concentrations (Fig. 6). If P_X/P_{Na} remains constant as the concentration of a test cation varies on the inside or outside, there should be a shift in V_{rev} of 17.9 mV (at 10°C) for a twofold change in cation concentration (activity). When internal $[K^+]$ or external $[Tl^+]$ was varied, however, the V_{rev} values determined by the experiments were not in accord with the predictions by Eq. 2 for the constant P_X/P_{Na}: the shifts were substantially less than 17.9 mV per twofold concentration change (Fig. 6, *B* and *D*).

The raise in internal $[K^+]$ led to the reduction in P_K/P_{Na}: $P_K/P_{Na} = 0.08$ for 160 mM internal K^+, and $P_K/P_{Na} = 0.15–0.16$ for a lower internal $[K^+]$ of 40 mM (Fig. 6 *C*). Similarly, P_{Tl}/P_{Na} substantially decreased as external $[Tl^+]$ increased (Fig. 6 *F*). The P_{Tl}/P_{Na} measured with external Tl^+ and internal Na^+ both at 80 mM (0.29) was far less than that measured at 10 mM (0.61), indicating that the concentration-dependent manner of P_{Tl}/P_{Na} is preserved even when internal $[Na^+]$ and external $[Tl^+]$ are symmetrically varied. For Rb^+ and Cs^+, the permeability ratio as determined from the biionic V_{rev} at 160 mM was less than the IUC ratio at 5 mM ($[I_X/I_{Na}]_5$) inferred from the IUC-concentration curve (see Table 3). This possibly reflects that P_{Rb}/P_{Na} and P_{Cs}/P_{Na} are decreasing functions of increasing external $[Rb^+]$ and $[Cs^+]$, respectively. In contrast, the P_K/P_{Na} measured with the fixed internal $[Na^+]$ was apparently invariant with changing external $[K^+]$. Thus, the concentration-dependent nature of the cardiac Na-channel selectivity was asymmetric with respect to both ion type and membrane surface.

Kinetic modeling of selective ion permeation in cardiac Na-channel

Development of dynamic pore model

A salient point in the experimental findings is that the biionic P_X/P_{Na} depends on concentrations of the permeant cations. Conventional static pore models ascribed the concentration-dependent P_X/P_{Na} to the asymmetric energy profile and multiple occupancy. However, we can propose an alternative hypothesis: permeant cations possibly induce a conformational transition of the Na-channel pore associated with a change in selectivity when they occupy a site in the permeation path, thereby causing the occupancy-dependent selectivity change. This mechanism would also yield the low K_m in IUC–concentration curves as for Tl^+, if the cation-induced conformational transition involves the increase in energy barriers for permeation of the cation on its own.

Based on these notions, we developed the dynamic pore model, assuming that the selectivity filter region of Na-channel pores exists in two conformational states, and examined how well the dynamic pore model accounts for the experimental findings as compared with the static pore model. As illustrated in Fig. 7, the dynamic pore mechanism involves the permeating cation (occupancy)-regulated transition between two conformations with different permeability properties, which are characterized by different energy profiles for each cation. According to this novel mechanism, the decrease in P_X/P_{Na} with increasing internal $[K^+]$ or external $[Tl^+]$, as well as the low K_m for Tl^+, is attributable to the cation concentration (occupancy)-dependent transition of Na-channel pores from one conformation with low Na^+ selectivity (high Tl^+ permeability) to the other with high Na^+ selectivity (low Tl^+ permeability).

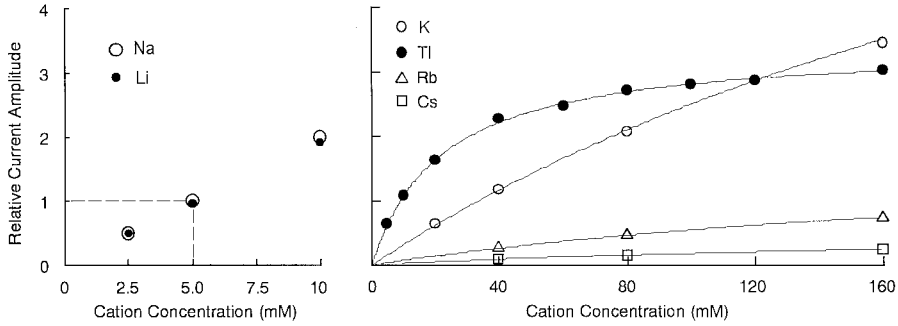

FIGURE 4 Peak IUC–concentration relationships for the monovalent metal cations. First, current recordings were performed with the control test solutions (160 mM Cs-, 160 mM Rb-, 40 mM KCl-, 5 mM Li-, 5 mM Na-, and 10 mM Tl-sol) in the same cell. Peak currents were normalized to the Na^+ current at 5 mM. Next, currents carried by each test cation at various concentrations were recorded in other cells, and then a peak current at each concentration was normalized to the current at the control concentration as given above for each test cation (e.g., 160 mM for Cs^+). The relative amplitude of current peaks at −20 mV was finally calculated as a ratio to the Na^+ current at 5 mM. The averaged values for individual test cations (n = 3–4) are plotted. The smooth curves are the best fits with Eq. 1.

We tested three subclasses of the dynamic pore model: 1) Model 1 (enzymatic transition), in which the conformational transition of the pore is strictly coupled with occupancy of the site by permeating cations, and so essentially deterministic (irreversible); 2) Model 2 (fluctuation-mode switch) involving random (reversible) fluctuations between two conformational states of the pore, the equilibrium of which shifts toward the Na^+-selective structure when a cation occupies the site within the pore; and 3) Model 3 (allosteric interaction), which requires an allosteric regulatory site located out of the restricted pore (e.g., in the vestibule). Basic state diagrams for these distinct model subtypes are depicted at the bottom of Fig. 7.

A set of the model parameters for Na^+, K^+, and Tl^+ was searched for each model subtype to reproduce all the experimental observations satisfactorily. For simplicity, we assumed the conformational transitions to be voltage independent, displacement of the binding site during the conformational transitions to be negligible (see Läuger, 1985), and occupancy of the site by 2 mM Ca^{2+} to be negligible at ≥ -20 mV.

Energy profiles for pore models to fit inward unidirectional current data

We first fitted the static and dynamic pore models to the IUC–concentration relationships and to I–V curves. In this study, we could not directly determine the energy profile for Na^+ as a reference cation because of the restriction of external [Na^+] to 10 mM. Therefore, the energy parameters for Na^+ translocation were somewhat arbitrarily set, according to the previous reports for cardiac Na-channels (Sheets et al., 1987; Nilius, 1988). As the initial step, the model parameters were adjusted for each test cation (K^+, Rb^+, Cs^+, Tl^+) by reconciling the theoretically computed K_m and $[I_X/I_{Na}]_5$ with the experimentally determined ones.

TABLE 3 Apparent dissociation constants and permeability ratios for monovalent metal cations

		Apparent Km (mM)					
Reference	Preparation	Na	Li	K	Rb	Cs	Tl
Present study	Guinea-pig ventricle			254	245	227	21.8
Hille, 1975	Frog sciatic nerve	368	165	220	220	220	50
Permeability relative to Na^+							
Present study 1*	Guinea-pig ventricle	1.0	0.96 (0.90)	0.17 (0.17)	0.037 (0.038)	0.013 (0.014)	0.63 (0.82)
Present study 2[#]	Guinea-pig ventricle	1.0	1.0 (0.94)	0.16 (0.16)	0.024 (0.025)	0.007 (0.008)	0.63 (0.82)
Sheets et al., 1987[§]	Canine cardiac Purkinje	1.0		0.094		0.02	
Hille, 1972	Frog sciatic nerve	1.0	0.93	0.086	<0.012	<0.013	0.33
Huang et al., 1979[¶]	Neuroblastoma (C9)	1.0		0.39	0.11	0.06	1.10

*IUC ratios at 5 mM. The data for K^+, Rb^+, and Cs^+ were derived from Eq. 1 as fitted to the IUC-concentration curves. The numbers in the parentheses represent the values corrected for the activity coefficients.

[#]Permeability ratios calculated from biionic V_{rev} using Eq. 2. The reference cation in the internal solution is Na^+ at 5 mM. The external concentrations of Li^+, K^+, Rb^+, Cs^+, and Tl^+ are 5, 40, 160, 160, and 5 mM, respectively. The data corrected for the activity coefficients are shown in the parentheses.

[§]Data from the measurement of biionic V_{rev}.

[¶]Data from the measurement of cation influx in the BTX-modified TTX-resistant Na-channel.

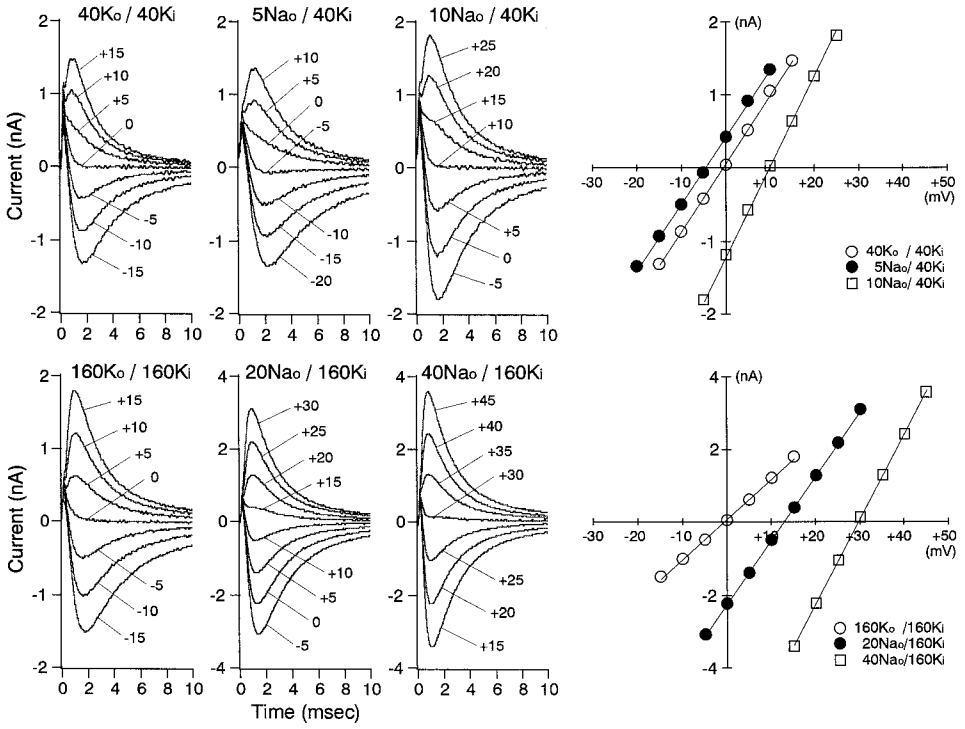

FIGURE 5 Measurement of biionic V_{rev} with 40 (*top*) or 160 (*bottom*) mM internal K^+ and 5–40 mM external Na^+. The traces show the capacity- and leak-corrected currents in response to test pulses separated by 5 mV near the reversal potential. Biionic conditions are indicated above each current family. The numbers for individual currents are the test potentials corrected for the liquid junction potentials (in mV). As shown on the extreme right, V_{rev} was determined by interpolating the peak I–V plots, which exhibited almost linear relation.

A parameter set that provides the most reasonable fit to the biionic P_X/P_{Na} data and to *I–V* curves was then selected for each model. The best-fit parameters for K^+ and Tl^+ (and Na^+) permeation in the 3B2S static and the dynamic pores are shown in Fig. 8. Also, the energy profiles of the symmetrical static pores to fit the IUC data for all the test cations (except Li^+) are listed in Table 4 for reference.

With the 3B2S static pore model, the energy profiles optimized for single- and double-occupancy pores were very similar, and the location of the rate-limiting barrier for Na^+ permeation little affected the determination of energy parameters for other test cations. The well depths for Tl^+ binding predicted by the static pore models were ≤ -4.3 *RT*, being lower than those previously determined for the binding of divalent metal cations such as Ca^{2+} (≥ -3.5 *RT*: see Yamamoto et al., 1984; Sheets et al., 1987), whereas the dynamic pore could have shallower wells.

Discrimination of pore models by biionic permeability ratio data

Figure 9 shows how well the biionic P_X/P_{Na} data fit the theoretical predictions by the two classes of pore model, the parameters of which were determined from the IUC data. We calculated the theoretical P_X/P_{Na} using the 3B2S static and the dynamic pore models with the parameter values selected for providing reasonable fit to the P_X/P_{Na} data, especially to the internal $[K^+]$- and external $[Tl^+]$-dependent decreases in P_X/P_{Na} (Fig. 8). The comparisons clearly support the choice of the dynamic pore model over the static pore model.

The symmetrical static pores were rejected because they predicted nearly concentration-independent P_X/P_{Na} or the increase in P_{Tl}/P_{Na} with increasing external $[Tl^+]$. The static single-occupancy pore with asymmetric energy profiles could qualitatively reproduce both internal $[K^+]$- and external $[Tl^+]$-dependent decrease in P_X/P_{Na}, but not compatible with either the external $[K^+]$-independent P_K/P_{Na} or the external $[Na^+]$-dependent increase in P_{Tl}/P_{Na}. For biionic conditions with a constant concentration ratio, static single-occupancy pore models always predict the concentration independent P_X/P_{Na} (Eisenman and Horn, 1983), whereas the biionic P_{Tl}/P_{Na} values experimentally determined for the symmetrical concentrations (Na^+ versus Tl^+) or fixed concentration ratios (Na^+ versus K^+) were concentration-dependent (Figs. 5 and 6 *F*). The introduction of multiion occupancy into the 3B2S model, with or without ionic repulsion, did not improve the fit to the P_X/P_{Na} data.

Of the dynamic pore model subtypes, Model 1 was considered the best for the following reasons: 1) Model 1 is the simplest version with the minimum number of free parameters. 2) According to classic thermodynamics, the principle of microscopic reversibility must be considered for reversible transitions as in Model 2; however, Model 2 failed to simulate the concentration-dependent P_X/P_{Na} when parameter values were limited by the principle of microscopic reversibility. 3) Model 1, with only one binding site in the pore, can fit the P_X/P_{Na} data more satisfactorily than Model 3, which requires two extra binding sites for internal K^+ and external Tl^+ (Fig. 9).

The concentration-dependent P_X/P_{Na} data demanded asymmetric energy profiles of the dynamic pore. Under

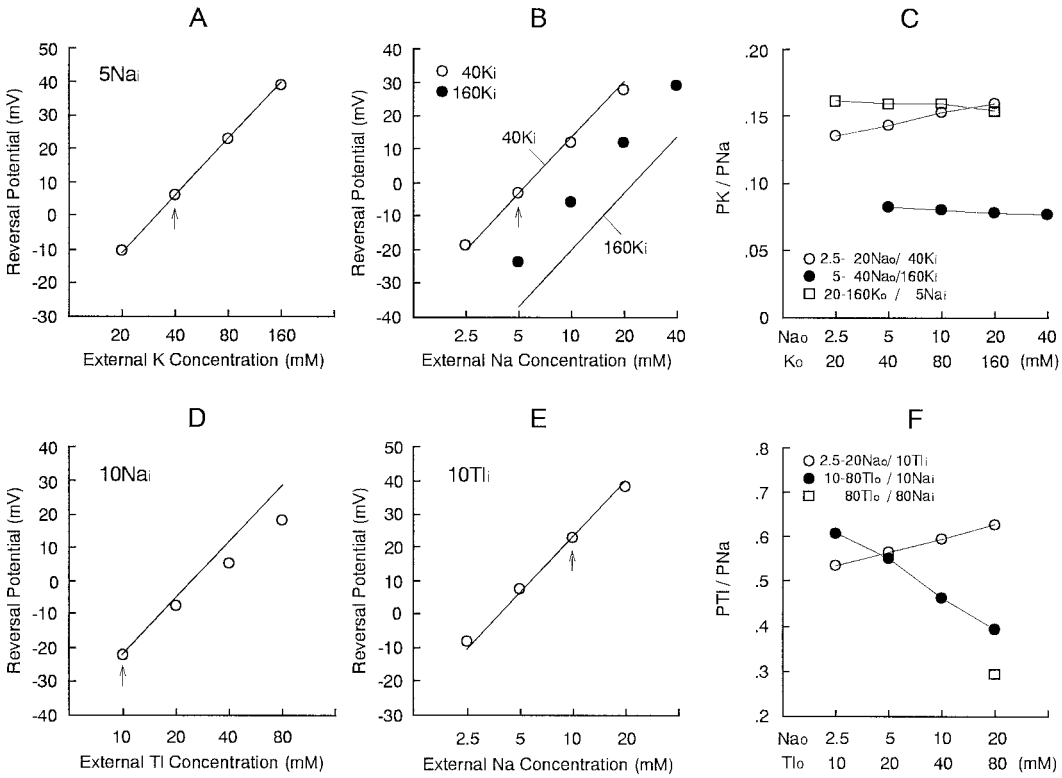

FIGURE 6 Biionic V_{rev} and P_X/P_{Na} determined under various biionic conditions. (A, B, D, E). The values of V_{rev} measured with fixed internal and varied external cation concentrations. Only the mean V_{rev} values (n = 3–4) are shown, because all the SEMs are within the size of the symbols. The solid lines have a slope of 17.9 mV per twofold change in the external cation concentration, designating the V_{rev} for the constant (concentration-independent) P_X/P_{Na} in Eq. 2; the arrows indicate the reference conditions to predict the V_{rev} values. (*C*, *F*) Concentration dependence of biionic P_X/P_{Na}. The values of P_X/P_{Na} for individual biionic conditions were computed with Eq. 2 and plotted against the concentrations of the external test cations.

symmetrical ionic conditions, both K^+ and Tl^+ currents exhibited the almost linear (ohmic) *I–V* relation in the potential range from −20 to +50 mV, whereas the *I–V* plots for symmetrical Na^+ (at 10 mM) revealed slight inward rectification at the potentials positive to +20 mV. Therefore, the energy profile for Na^+ was assumed to be asymmetric, and those for Tl^+ and K^+ nearly symmetric. The inward rectification of Na^+ currents required the external barrier to be lower than the internal one. The rate constant α_{Na} was somewhat arbitrarily set at a lower value (ΔG_α =

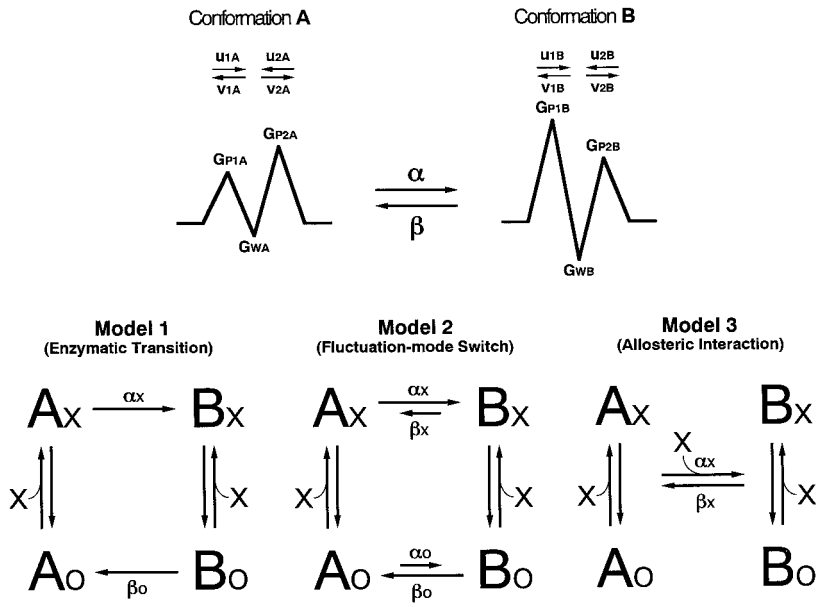

FIGURE 7 Minimal dynamic pore schemes for the cardiac Na-channel. (*Top*) Schematic diagrams of the dynamic pore existing in two conformational states, **A** and **B**, with the 2B1S energy profiles for ion passage. The rate constants for the conformational transition are denoted α and β. (*Bottom*) State diagrams describing the states of occupancy and possible transitions between the states for three distinct dynamic pore mechanisms, enzymatic transition (Model 1), fluctuation-mode switch (Model 2), and allosteric interaction (Model 3). In the presence of only one permeant cation species, the four allowed states are assigned for the cation–pore interaction. The subscripts O and X represent the empty pore and the pore occupied by the permeant cation X^+, respectively.

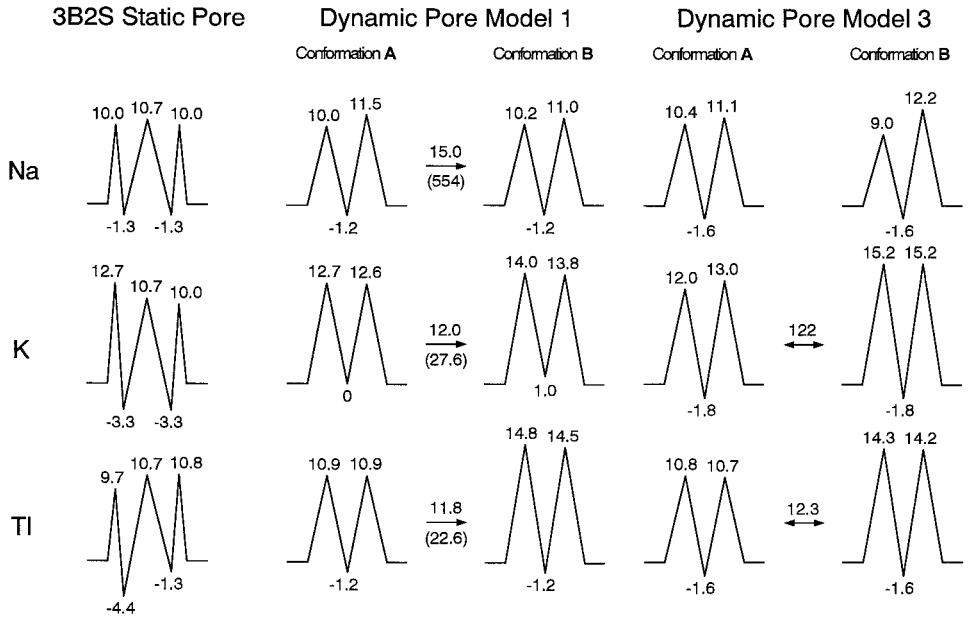

FIGURE 8 Best-fit parameters for the dynamic pores (Models 1 and 3) and for the 3B2S static pore. The parameter values were determined for each model to mimic the kinetic properties of the Na-channel including the biionic P_X/P_{Na} and *I–V* relation. The energy profiles for Na^+, K^+, and Tl^+ (at 0 mV) are shown by the numbers in RT units on individual energy diagrams. The rate constants for the transition from **A** to **B** in Model 1 are given as activation energy in RT units (i.e., ΔG_α in Eq. A21), and the time constants ($1/\alpha$ in ns) are also shown in the parentheses. The time constant for the backward transition from **B** to **A** ($1/\beta$) was adjusted to 1000 ns ($\Delta G_\beta = 15.6\ RT$). The dissociation constants (β/α) for binding K^+ and Tl^+ (in mM) are shown for Model 3.

15.0 *RT*), because the rapid transition in the Na^+-occupied states yielded the $[Na^+]$-dependent reduction in P_X/P_{Na}. (cf. Fig. 6, *C* and *F*).

Effects of vestibule surface charge on selective permeability of static pore

The vestibule surface potential V_S is known to affect the permeability and selectivity of Na-channels; therefore, static pores linked with charged vestibules (i.e., static pore models with variable V_S) may possibly account for the concentration-dependent P_X/P_{Na} data. In Fig. 10, the effects of V_S and cation binding to the surface charge on P_X/P_{Na} are shown for the 3B2S static pore. The external and internal V_S certainly affected P_X/P_{Na} for the asymmetrical static pore. However, the fit to the external $[Tl^+]$- and internal $[K^+]$-dependent P_X/P_{Na} was not improved by incorporating the surface charge binding effects of external Tl^+ and internal K^+ (Fig. 10, *bottom*). In conclusion, the vestibule surface charge did not enable the static pore model to provide reasonable fit to the P_X/P_{Na} data from the cardiac Na-channel.

Permeability properties of cardiac Na-channel as dynamic pore

The permeability properties of the cardiac Na-channel, as described by Model 1, are characterized as follows (see Fig. 8): 1) Conformation **A** has relatively low Na^+ selectivity, whereas conformation **B** is highly Na^+-selective. The selectivity sequence as determined from biionic P_X/P_{Na} is $Na^+ \approx Tl^+ > K^+$ for **A**, and $Na^+ \gg K^+ > Tl^+$ for **B**. 2) The pore has relatively shallow wells for Tl^+, the depth of which can be equal to that for Na^+. The low K_m for Tl^+ is ascribable to the concentration-dependent shift in the distribution between **A** and **B** to favor the latter (with lower Tl^+

TABLE 4 Best-fit energy parameters for static pore models

Reference	Pore Model		Energy Profiles (RT)					
			Na	Li	K	Rb	Cs	Tl
Present study*	2B1S	Peaks	10.8	10.9	12.6	14.1	15.1	10.8
		Well	−1.8		−2.2	−2.3	−2.4	−4.9
	3B2S[#]	Side Peaks	9.0	9.0	9.0	9.0	9.0	9.0
	Central	Peak	11.3	11.4	13.2	14.8	15.8	11.3
			(11.4)	(11.5)	(13.3)	(14.8)	(15.9)	(11.4)
		Wells	−1.2		−1.5	−1.6	−1.7	−4.3
			(−1.1)		(−1.5)	(−1.6)	(−1.7)	(−4.3)
Hille, 1975[§]	4B3S	Peak	9.0	9.1	11.7	>13.7	>13.7	10.4
		Well	−1.0	−1.8	−1.5	−1.5	−1.5	−3.0

*Energy parameters for symmetrical pores were determined from the IUC data.

[#]Binding of permeant cations to the outer and inner sites was assumed to be diffusion limited. The energy values are shown for the single-occupancy pore, and also for the double-occupancy pore (no ionic repulsion) in the parentheses.

[§]For comparison, the data for the neuronal TTX-sensitive Na-channel are shown. The energy values for the rate-limiting barrier (Peak) and the outermost binding-site (Well) of the 4-barrier 3-site single-occupancy pore were determined from the peak *I–V* and V_{rev} data.

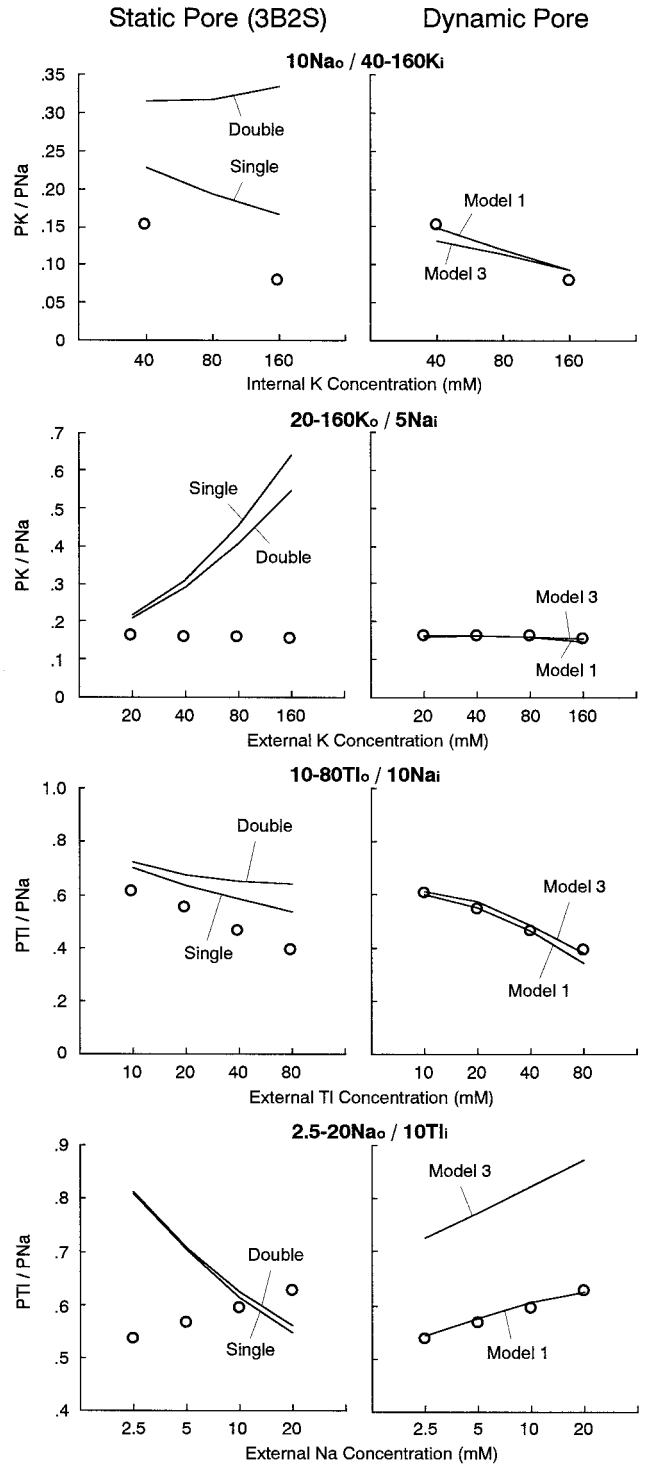

FIGURE 9 Prediction of biionic P_X/P_{Na} by the 3B2S static pore and the dynamic pore models. Theoretical V_{rev} for various biionic conditions was determined by calculating *I–V* relations for the model pores with the best-fit parameters, then P_X/P_{Na} was derived from Eq. 2. The continuous lines show the theoretical P_X/P_{Na} predicted by the 3B2S static (single- and double-occupancy) pores and the dynamic pores (Models 1 and 3). The experimental data are also plotted for comparison (*open circles*). Biionic conditions are indicated above each panel. The data for the symmetrical static pores and Model 2 are not shown, because they did not exhibit the concentration dependence as observed in the experiments.

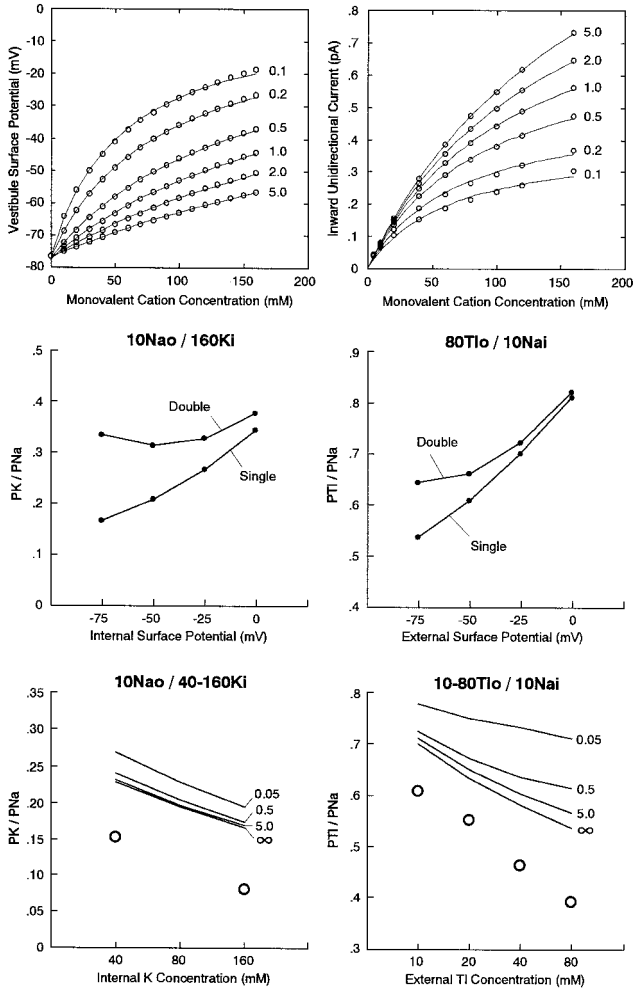

FIGURE 10 Influences of vestibule surface potentials on the biionic selectivity of the 3B2S static pore linked with charged vestibules. (*Top-left*) Decrease in V_S by binding of monovalent cations to a fixed negative charge with different K_D values. The V_S at various concentrations of a binding cation was calculated for a given K_D using the GCS analysis. The control V_S for infinite K_D (or in the absence of binding cations) was -76.6 mV. The smooth curves labeled by the K_D values (in M) are the best fits with the Langmuir isotherm. (*Top-right*) IUC-concentration curves predicted for the different K_D values. Amplitude of IUCs carried by Na^+ in a single Na-channel (at -20 mV) was computed from the single-occupancy pore model with the energy profiles shown in Fig. 8, and plotted for individual K_D values. The smooth curves are the best fits with Eq. 1. (*Middle*) Dependence of theoretical P_X/P_{Na} on the external or internal V_S. The continuous lines show the P_X/P_{Na} predicted by the single- and double-occupancy pores with the best-fit parameters. V_{rev} was determined from the simulated *I–V* relation, then P_X/P_{Na} was calculated with Eq. 2. The V_S values in both vestibules were first set equal to -75 mV as a control, and one of them was reduced to -50, -25, and then 0 mV. (*Bottom*) Effects of cation binding to the surface charge on the concentration dependence of P_X/P_{Na}. The continuous lines are the theoretical predictions by the charged vestibule model with the K_D values 0.05, 0.5, 5.0 M and infinity (∞). The control V_S in either side was assumed to be -75 mM. The experimental data are also plotted for comparison (*open circles*).

permeability). 3) The transition rate constant α_X depends on permeant cation species. The order of efficacy in facilitating the transition is $Tl^+ \geq K^+ > Na^+$; thus, relatively imper-

meant cations are possibly more efficacious than the highly permeant cation Na^+. 4) Native Na-channel pores undergo conformational transitions on a time scale of nanosecond order during cation permeation. These very fast transitions would not be detectable in the single-channel recording for which the theoretical lower limit of temporal resolution is of the order of 10 μs (Läuger, 1985).

Model 1 could clearly describe the mechanisms of the concentration-dependent selectivity changes as well as the low K_m for Tl^+ in IUC–concentration relation. Figure 11 shows the concentration-dependent kinetics of the dynamic pore and carried IUCs in the presence of external K^+ or Tl^+ alone. As external $[K^+]$ or $[Tl^+]$ increases, the steady-state probability of **A** decreases while that of **B** increases. It is evident that K_m for IUC–concentration relation of the dynamic pore is affected by the concentration-dependent transition from **A** to **B**. The K_m predicted for Tl^+ currents is relatively low as observed in the experiments, because Tl^+ induces the conformational transition to the Tl^+ impermeable form **B**. As shown in Fig. 12, the concentration-dependent P_X/P_{Na} in the dynamic pore is attributable to the combined effects of the cation occupancy-induced transition to **B** with lower P_X/P_{Na} and the asymmetric energy profile for Na^+ yielding the concentration-dependent change in the P_X/P_{Na} of **A**. The external $[K^+]$-dependent increase in the P_K/P_{Na} of **A** was offset by the transition to **B** with lower P_K/P_{Na}. This explains why P_K/P_{Na} is apparently independent of the external $[K^+]$.

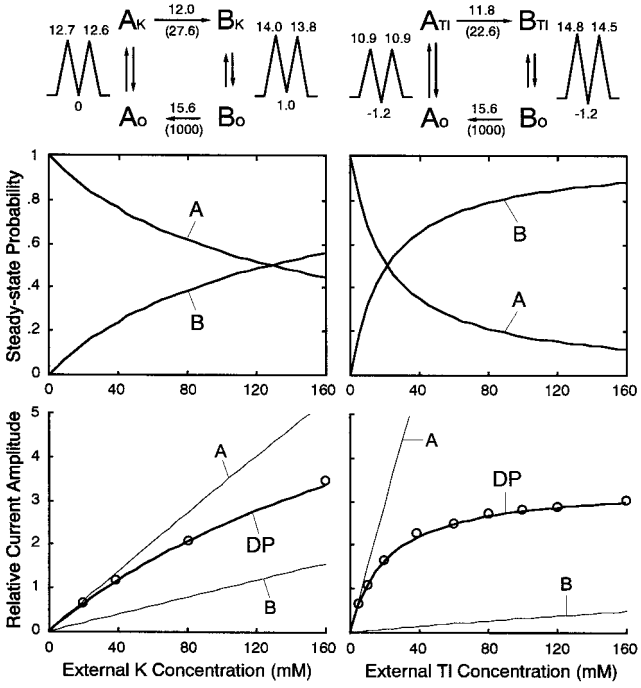

FIGURE 11 Concentration-dependent kinetic behavior of Model 1 and carried IUCs in the presence of K^+ (*left*) or Tl^+ (*right*) only on the outside. (*Top*) State diagrams with the best-fit parameters. (*Middle*) Steady-state probabilities of **A** and **B** during the inward unidirectional passage of K^+ or Tl^+ at various external concentrations. (*Bottom*) Simulated IUC-concentration curves for K^+ and Tl^+. Amplitude of IUCs at −20 mV was calculated for the concentrations experimentally tested (≤160 mM), then normalized to the Na^+ current at 5 mM (cf. Fig. 4). The continuous lines labeled DP are the scaled predictions by the dynamic pore, being well approximated by Eq. 1 with the K_m of 253 mM for K^+, and 21.5 mM for Tl^+. The experimental data are superimposed for comparison (*open circles*). Current–concentration curves for the pore fixed in **A** and **B** are also shown by the continuous lines labeled A and B, respectively.

DISCUSSION

Relationship between cation permeation and gating mechanisms

The voltage-dependent gating parameters exhibited the hyperpolarizing and depolarizing shifts during the consecutive perfusions of different external test solutions. The depolarizing shift is known to reflect the surface charge effects of cations (Makielski et al., 1987; Hanck and Sheets, 1992b), whereas the hyperpolarizing shift corresponds to the spontaneous negative shift in Na-channel kinetics (Kimitsuki et al., 1990; Hanck and Sheets, 1992a). According to Dani (1986), large organic cations are less effective in screening vestibule surface charges than smaller metal cations; replacement of TMA molecules ($\varnothing \approx 6.0$ Å) by group Ia cations ($\varnothing = 1.56$–3.30 Å) is expected to diminish V_S (by 10–20 mV for the total substitution of 150 mM). Thus, the size effect of cations on the vestibule surface charge screening may partly contribute to the depolarizing shift in gating kinetics.

Only Tl^+ induced the significant depolarizing shifts in the kinetic parameters (see Figs. 2 and 3). These positive shifts would not be due to the surface charge screening effect of Tl^+ in the external vestibule because the replacement of TMA by the smaller cation K^+ only caused slight depolarizing shifts. The concentration-dependent parallel shifts in Tl^+ current kinetics suggest the surface charge binding effect of external Tl^+ rather than a direct effect on the gating machinery.

Hille (1972) reported that the voltage dependence of Na-channel activation shifted to the depolarizing direction by a few millivolts when external Na^+ (at 110 mM) was replaced by other monovalent cations such as K^+. This positive shift in the activation kinetics could not be ascribed to the surface charge effects because there were no significant changes in either the steady-state availability or the inactivation time constant. Similarly, Yamamoto et al. (1985) showed that the gating kinetics of squid axon Na-channels is appreciably affected by permeant cation species. The permeant ion-dependent gating behavior has also been demonstrated for Ca- and K-channels (Matteson and Swenson, 1986; Shuba et al., 1991; Demo and Yellen, 1992; Gómez-Lagunas and Armstrong, 1994; Kiss and Korn, 1998), the previous reports suggesting that occupancy of binding-sites by cations affects gating kinetics. In contrast to the report by Hille (1972), however, no comparable effects of external K^+ on activation or other kinetic parameters were observed in this study. Within the concentration range tested (≤160 mM), the cardiac Na-channel gating

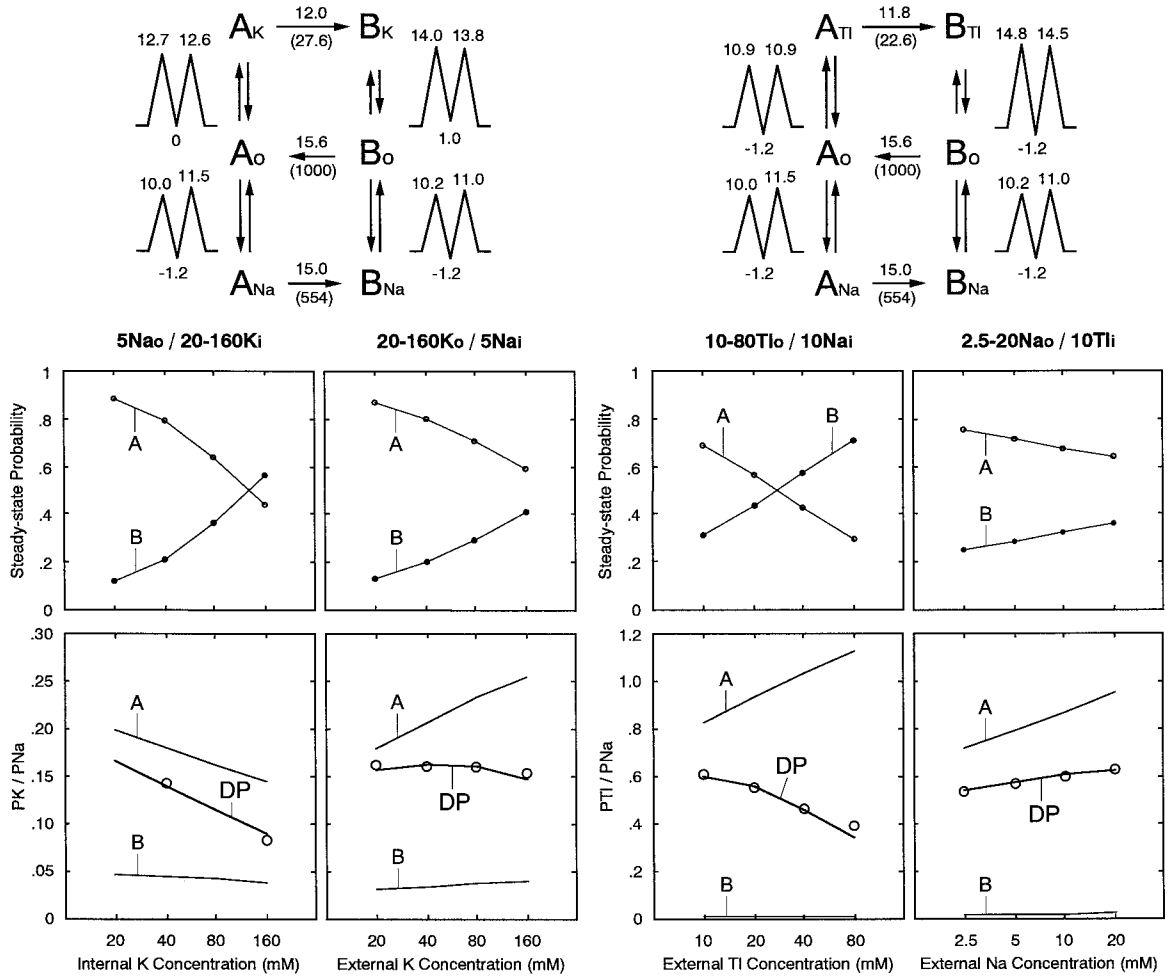

FIGURE 12 Mechanisms of the concentration-dependent selectivity changes as described by Model 1. (*Top*) State diagrams describing the permeation kinetics in the presence of two permeant cations, Na^+ and K^+ (*left*), or Na^+ and Tl^+ (*right*). (*Middle*) Steady-state probabilities of **A** and **B** under the different biionic conditions shown above the panels. The state probability at V_{rev} was computed for each biionic condition, and plotted against the concentrations of the test cations. (*Bottom*) Theoretically predicted P_X/P_{Na} for the dynamic pore (labeled DP) and for the pore fixed in **A** and **B** (labeled A and B, respectively). The biionic P_X/P_{Na} was determined from V_{rev} in the simulated *I–V* plot using Eq. 2. The experimental data are also shown for comparison (*open circles*).

appeared to be independent of permeant cation species as well as concentrations on the outside.

Selective permeability of cardiac TTX-insensitive Na-channel

Cardiac Na-channel is substantially permeable to Rb^+ and Cs^+

It has been reported that native TTX-sensitive Na-channels are not measurably permeable to either Rb^+ or Cs^+ (Hille, 1972, 1975; Ebert and Goldman, 1976). In contrast, the present study, in which Rb^+ and Cs^+ currents flowing through the Na-channel were directly recorded as IUCs, demonstrated that the native cardiac Na-channel is substantially permeable to both Rb^+ and Cs^+ (see Fig. 1). There are few available data for comparison on the selectivity of native TTX-insensitive Na-channels. However, a report from the biionic V_{rev} measurement for canine cardiac Purkinje cells provided a P_{Cs}/P_{Na} value of 0.020 (Sheets et al., 1987), which is close to (slightly bigger than) those determined in this study (see Table 3). These data possibly indicate that cardiac TTX-insensitive Na-channels are less selective to Na^+ and more permeable to both Rb^+ and Cs^+ than TTX-sensitive ones.

Huang et al. (1979) compared the selectivity of BTX-activated Na-channels for alkali cations in two neuroblastoma cell lines, N18 (TTX-sensitive) and C9 (TTX-resistant). Although there was no qualitative difference in the selectivity sequence, the relative permeability to K^+, Rb^+, and Cs^+ of the TTX-resistant channel was a little greater than that of the TTX-sensitive isoform. That report, together with our finding, implies that the relatively low selectivity of TTX-insensitive Na-channels is a general property of the Na-channel family, which holds even after BTX treatment. It is not reasonable to compare our data with those obtained from the single-channel recordings for toxin-modified Na-

channels because the treatment with toxins such as BTX is known to change the conductivity and selectivity of Na-channels (Khodorov, 1985; Garber and Miller, 1987; Green et al., 1987).

Thallous ion is highly permeant with apparently high affinity

Compared with group Ia cations, Tl^+ apparently exhibited the high affinity (low K_m) for the cardiac TTX-insensitive Na-channel and for the neuronal TTX-sensitive one (Table 3). Hille (1972) suggested that Tl^+ can bind to a site more tightly than any group Ia cations because of its highly polarizable outer electron shells. This specific property of Tl^+ to lower an energy profile for its permeation may, in part, contribute to the low K_m in IUC-concentration relation and the high permeation rate at low concentrations.

We estimated the P_{Tl}/P_{Na}, corrected for the activity coefficients, to be 0.38–0.82 with 10–80 mM Tl^+ outside, and 10 or 80 mM Na^+ inside. These P_{Tl}/P_{Na} values are greater than that determined for the neuronal TTX-sensitive Na-channel from the biionic V_{rev} measurement with both external Tl^+ and internal Na^+ at 110 mM (0.33, Hille, 1972). However, the difference in P_{Tl}/P_{Na} between the two subtypes may result from the difference in the cation concentrations used because P_{Tl}/P_{Na} has been shown to depend on both [Na^+] and [Tl^+], and the P_{Tl}/P_{Na} values for an external [Tl^+] of 80 mM in the cardiac Na-channel (0.38–0.51) were close to that for 110 mM external Tl^+ in the neuronal one (0.33). High permeability to Tl^+ with apparently low K_m may be a common property of Na-channels without respect to TTX sensitivity.

Biionic permeability ratio is concentration- and orientation-dependent

Consistent with our findings, the P_K/P_{Na} determined from biionic V_{rev} for TTX-sensitive Na-channels increased as internal [K^+] reduced (Cahalan and Begenisich, 1976; Ebert and Goldman, 1976). Hence, the concentration-dependent P_X/P_{Na} would be, regardless of TTX sensitivity, a general feature in Na-channel selectivity. The previous studies for TTX-sensitive isoforms further showed the decrease in P_K/P_{Na} with increasing internal [Cs^+] or [Rb^+] (Ebert and Goldman, 1976; Begenisich and Cahalan, 1980a). These observations established that internal K^+, Rb^+, and Cs^+ increase the selectivity of Na-channels to Na^+. In contrast, it was controversial whether external permeant cations affect the Na-channel selectivity: Begenisich and Cahalan (1980a) reported that the changes in the external cation concentrations gave the expected shifts for a constant P_X/P_{Na}; in another report by Yamamoto et al. (1985), the biionic P_X/P_{Na} also depended on the external cation concentrations (with a fixed internal [Na^+]). In this study, the P_X/P_{Na} depended not only on the internal [K^+] but also on the external [Tl^+] and [Na^+], verifying that both internal and external cations can affect the Na-channel selectivity (Fig. 6).

Possible influence of internal TMA block on permeability data

Internal TMA is known to cause a voltage-dependent block of Na-channels (Horn et al., 1981; Oxford and Yeh, 1985; O'Leary and Horn, 1994); therefore, TMA used for internal solutions may affect estimation of permeation kinetics. In our experiments, the Na^+ current–voltage relation determined at a symmetrical concentration of 10 mM ([TMA] = 150 mM) showed slight inward rectification, possibly reflecting the blocking effect of internal TMA. Nevertheless, we assumed that the internal TMA block is negligible, and the inward rectification of Na^+ currents is chiefly due to the asymmetric energy profile of the pore for Na^+, because the current–voltage relations for symmetric 10 mM Tl^+ (150 mM TMA) and 40 mM K^+ (120 mM TMA) were almost linear, and because the asymmetric energy profiles for Na^+, which were required for reproducing the P_X/P_{Na} data, could also predict the inward rectification of Na^+ current–voltage relation without involving the TMA block.

Assuming that the internal TMA block causes the inward rectification of Na^+ currents, a dissociation constant at 0 mV [$K_B(0)$] for TMA is estimated to be 670 mM, much greater than that reported previously (≤370 mM: O'Leary and Horn, 1994). According to the dynamic pore model, the internal TMA block with a $K_B(0)$ of 670 mM would raise the apparent K_m of IUC-concentration relations by 1.1–5.1%, and would reduce the maximum IUC to 0.91–0.94 of the control (without TMA block); V_{rev} and P_X/P_{Na} are independent of the TMA block. Thus, the blocking effect of internal TMA on the guinea pig heart Na-channel appears to be relatively weak, and the influence of the TMA block on the selectivity analyses would be small.

Mechanisms of selective ion permeation in Na-channel

Biionic permeability ratio data support dynamic pore model

Various types of static pore models have been used to describe permeability properties of an open channel: 2B1S, 3B2S (single- or multi-ion occupancy) and four-barrier three-site (4B3S) models (e.g., Hille, 1975; Begenisich and Cahalan, 1980a,b; Garber, 1988; Naranjo and Latorre, 1993; Pérez-Cornejo and Begenisich, 1994; Wells and Tanaka, 1997). The early theories assumed single-ion occupancy at a time (Hille, 1975; Yamamoto et al., 1984; Sheets et al., 1987). For biionic conditions of symmetrical concentrations or a constant concentration ratio, the one-ion pores, the P_X/P_{Na} of which depends only on the peak energy differences between two permeant species, always predict the concentration-independent P_X/P_{Na}. As shown in Fig. 9, however, when only the external cation concentration is varied with a fixed internal concentration, the single-occupancy pore with asymmetric energy profiles can yield apparent (not true) concentration dependence of P_X/P_{Na}, which is actually due to the voltage-dependent shift in the

location of rate-determining barriers for different species (see Eisenman and Horn, 1983; Garber, 1988). Nevertheless, the asymmetric single-occupancy pore could not duplicate the P_X/P_{Na} data presenting the orientation-dependent nature. This inconsistency is further supported by the fact that the P_X/P_{Na} determined with a fixed concentration ratio was still concentration-dependent (see Figs. 5 and 6). More recent works using static pore models focused on the multi-ion pore with ionic repulsion, and the ionic composition-dependent P_X/P_{Na} has been interpreted as a consequence of the multiple occupancy (e.g., Begenisich and Cahalan, 1980a). In this study, however, the 3B2S double-occupancy pore failed to fit the biionic P_X/P_{Na} data (see Fig. 9, *left*).

In contrast to the static pore models, Model 1 could quantitatively reproduce all the P_X/P_{Na} data (see Fig. 9, *right*). This novel mechanism ascribes the concentration-dependent P_X/P_{Na} to the cation occupancy-induced transition of Na-channel pores from the Na^+-nonselective to Na^+-selective conformation. In this study, only K^+ and Tl^+ were tested (as cation X^+); however Rb^+, Cs^+, and other inorganic and organic cations have also been reported to affect biionic P_X/P_{Na} (Cahalan and Begenisich, 1976; Ebert and Goldman, 1976; Begenisich and Cahalan, 1980a; Yamamoto et al., 1985). The conformational transition of Na-channel pores to a Na^+-selective form may be a general mechanism underlying the cation-induced selectivity changes without respect to the type of monovalent cations. The P_K/P_{Na} measured with a fixed internal $[Na^+]$ can be apparently independent of the external $[K^+]$, when the external $[K^+]$-dependent conformational transition to the Na^+-selective structure offsets the external $[K^+]$-dependent increase in the P_K/P_{Na} of the Na^+-nonselective form resulting from the asymmetric energy profile for Na^+ (Fig. 12). This suggests that very careful and accurate determination of P_X/P_{Na} is required for exploring whether the concentration-dependent P_X/P_{Na} arises from a conformational transition between different selectivity states, or from other mechanisms such as asymmetric energy profiles, multi-ion occupancy and surface charge effects.

We assumed the 2B1S energy profile for cation transfer in the dynamic pore; this simplistic single-site pore provided the satisfactory fit to the experimental data obtained in this study. However, the previous reports suggested that there are two cation binding sites in Na-channel pores, thus the 3B2S energy profile may be the minimal scheme (Green et al., 1987; French et al., 1994). In the 3B2S pore, a probability of each site to be occupied under biionic conditions can be theoretically shown to depend on the orientation of permeant cations: fractional occupancy of the inner site by K^+ is nearly proportional to the internal $[K^+]$ (with a fixed external $[Na^+]$), whereas the external K^+ (at $\leq$160 mM) yields less occupancy of the inner site. This suggests an alternative explanation for the orientation-dependent P_K/P_{Na}. If only the inner site in the 3B2S pore is responsible for the occupancy-dependent conformational transition, P_K/P_{Na} would depend on the internal $[K^+]$ but not on the external $[K^+]$ ($\leq$160 mM). This is analogous to the gating-site occupancy hypothesis proposed for K-channels (Matteson and Swenson, 1986; Demo and Yellen, 1992). Further experiments may demonstrate that two binding sites inside the pore are required for describing permeability properties of Na-channels.

Characterization of dynamic pore mechanism

The static pore is characterized by the rigid structure of the selectivity filter region or the very rapid (quasi-instantaneous) rearrangement of ligands after an ion jump, providing a time-independent energy profile for a given occupancy state. By current concepts of the protein dynamics, however, the existence of multiple conformational substates and internal motions at a wide time range (from side-chain realignment on a picosecond time scale to large folding transition occurring over microseconds to seconds) have been suggested for biological proteins including ionic channels (see Läuger, 1985). In a recent study, the molecular motions of the flexible *P*-loops forming the pore constriction, which involve the backbone distortion of several angstromes, have been demonstrated for cloned Na-channels (Bénitah et al., 1997), indicating that the selectivity filter region of Na-channel pores can undergo conformational transitions that are relatively slow as compared with ion translocation in the pore. Furthermore, Tsushima et al. (1997a,b) reported that flexibility of the Na-channel *P*-loops might be essential to the selective Na^+ permeation. These findings suggest that the concentration-dependent selectivity changes are due to the structural transition of the pore between multiple conformations with different selectivity properties, the kinetics of which is regulated by the interactions between polar groups of the channel protein and permeant cations bound on the site in the pore or vestibule (see Mironov, 1992). The dynamic pore model elaborated in this study would provide a quantitative basis to this hypothesis. A very similar mechanism (essentially the same as Model 1) was suggested previously as the site-controlling selectivity hypothesis (Cahalan and Begenisich, 1976; also see Ebert and Goldman, 1976).

Original ideas and theoretical aspects of ion permeation through open channels existing in multiple conductive states were first given by Läuger et al. (1980) as the fluctuating-barrier model (also see Läuger, 1985; Heinemann and Sigworth, 1990; Dani and Fox, 1991; Moss and Moczydlowski, 1996), which corresponds to Model 2 (fluctuation-mode switch mechanism). With the principle of microscopic reversibility applied, however, Model 2 could not simulate the concentration-dependent P_X/P_{Na}. The recent studies for Ca- or K-channels have proposed several permeation models involving conformational transitions, the manners of which are different from the fluctuating-barrier mechanism (e.g., Lux et al., 1990; Draber et al., 1991; Mironov, 1992). Based on the kinetic features of the enzyme catalysis, Mironov (1992) proposed a conformational model describing the irreversible state transition coupled with cation binding, like Model 1. As suggested previously, the principle of microscopic reversibility is not applicable to these irreversible transition models (Lux et al., 1990; Mironov, 1992). However, the selectivity filter of ion channels is analogous to the active site of enzymes, and so describing an ion channel as

an enzyme, *permease*, would be useful in providing a conceptual framework to characterize channel–ion interactions (see Garber, 1988; Eisenberg, 1990; Richard and Miller, 1990; Tsushima et al., 1997b). Because the enzyme kinetics is considered as essentially irreversible, a kinetic model involving irreversible transitions is probably suitable for describing channel behavior.

A salient feature of our model for the Na-channel is that the conductivity and binding affinity to the physiological ion Na^+ vary little during the conformational transition, whereas most of the previous models described the transitions involving changes in conductivity and/or binding affinity to physiological ions. This feature of the Na-channel model is analogous to that of gramicidine A channels, which undergo structural fluctuations on a time scale of picoseconds to microseconds with the rate of the NH_4^+ entry unchanged (see Heinemann and Sigworth, 1990, 1991).

The previous models describing conformational transitions of channel pores involved inevitable duality in the classification of the permeation process versus gating process, that is, the coupling between ion occupancy and gating (e.g., Eisenman and Horn, 1983; Lux et al., 1990; Moss and Moczydlowski, 1996). In contrast, the conformational transition of the Na-channel pore, having been shown not to affect the gating kinetics, can be clearly distinguished from the gating process.

Possible implications and significance of the dynamic pore model

It is known that the Na-channels treated with alkaloid neurotoxins are less selective to Na^+ and more permeable to larger cations than the normal (toxin-unmodified) counterparts (Huang et al., 1979; Khodorov, 1985; Garber and Miller, 1987; Green et al., 1987). Huang et al. (1979) suggested that BTX directly modifies the steric structure of the selectivity filter region thereby increasing the minimum dimension of the pore. According to the dynamic pore model, however, a change in Na-channel selectivity can result from a shift in distribution between different selectivity states. The BTX-treated Na-channels have the selectivity sequence $Tl^+ \geq Na^+ > K^+$ (see Tables 1 and 3 in Huang et al., 1979; Table 2 in Khodorov, 1985), which is very similar to that for the Na^+-nonselective conformation of the dynamic pore (Fig. 12); whereas native Na-channels have the sequence $Na^+ > Tl^+ > K^+$. Furthermore, BTX and aconitine have been reported to raise the apparent K_m for Tl^+ as well as increasing the P_{Tl}/P_{Na} (Mozhayeva et al., 1977; Khodorov and Revenko, 1979). Therefore, the toxin-induced reduction in the selectivity to Na^+ may be in part ascribable to an inhibition of the transition to the Na^+-selective form. If this is the case, a study using the toxins would miss the essential permeability property of native Na-channels, which is characterized by small dynamic motions of the pore during cation transfer. Measurement of concentration dependence of biionic P_X/P_{Na}, as well as Tl^+ current–concentration relation, for toxin-modified channels would allow us to test this hypothesis.

The dynamic pore model suggests the flexible structure of channel pores separated from gating machinery. We have reported that group IIb cations (Zn^{2+}, Cd^{2+}, Hg^{2+}) block Na-channel currents without affecting the gating kinetics via conformational transitions of the permeation path (Kurata et al., 1998; also see Visentin et al., 1990; Sheets and Hanck, 1992). Furthermore, effects of channel-blocking compounds have been shown to depend on permeating ions (e.g., Ikeda and Korn, 1995). These findings reflect conformational flexibility of permeation pathways (i.e., allosteric interactions between the binding sites for permeant ions inside the pore and those for blocking compounds). Channel pore flexibility has also been supported by the observations of subconductance states (e.g., Schild et al., 1991; Ravindran et al., 1991; Schild and Moczydlowski, 1994; Moss and Moczydlowski, 1996). Dynamic behavior of channel pores may be, regardless of channel types, a general mechanism underlying the diverse modifications of ion channel permeability, such as the permeant ion-dependent selectivity change, toxin-induced selectivity change, permeating ion-dependent block, and substate formation.

APPENDIX

Energy profiles for ion translocation in model pores

General Gibbs free energy profiles for (ion-unoccupied) 2B1S and 3B2S pores are depicted in Fig. A1. All the effective V_m was assumed to fall across the narrow region of the pores (i.e., $D_{S1} = 0$, $D_{S2} = 1$), and all the energy peaks were placed equidistant between adjacent energy minima. The electrical distances of the energy peaks and wells (distance parameters) preset for the 2B1S pore were $D_{P1} = 0.25$, $D_{P2} = 0.75$, and $D_W = 0.5$; those for the 3B2S pore were fixed at $D_{P1} = 0.1$, $D_{P2} = 0.5$, $D_{P3} = 0.9$, $D_{W1} = 0.2$, and $D_{W2} = 0.8$, according to Schild and Moczydlowski (1994).

Mathematical formulation of ion translocation in model pores

Total free energies

For the energy profiles with the electric environment drawn at the bottom of Fig. A1, the energy level at a peak (E_{Pi}), at a well (E_{Wi}) or in a channel vestibule (E_{Si}) is expressed as a sum of the chemical and electrostatic terms,

$$E_{Pi} = G_{Pi} + D_{Pi} \cdot V_m + V_{Pi}$$
$$V_{Pi} = \frac{(D_{S2} - D_{Pi}) \cdot V_{S1} + (D_{Pi} - D_{S1}) \cdot V_{S2}}{D_{S2} - D_{S1}} \quad \text{(A1)}$$

$$E_{Wi} = G_{Wi} + D_{Wi} \cdot V_m + V_{Wi}$$
$$V_{Wi} = \frac{(D_{S2} - D_{Wi}) \cdot V_{S1} + (D_{Wi} - D_{S1}) \cdot V_{S2}}{D_{S2} - D_{S1}} \quad \text{(A2)}$$

$$[E_{S1}, E_{S2}] = [\ln(a_{ex}), \ln(a_{in}) + V_m], \quad \text{(A3)}$$

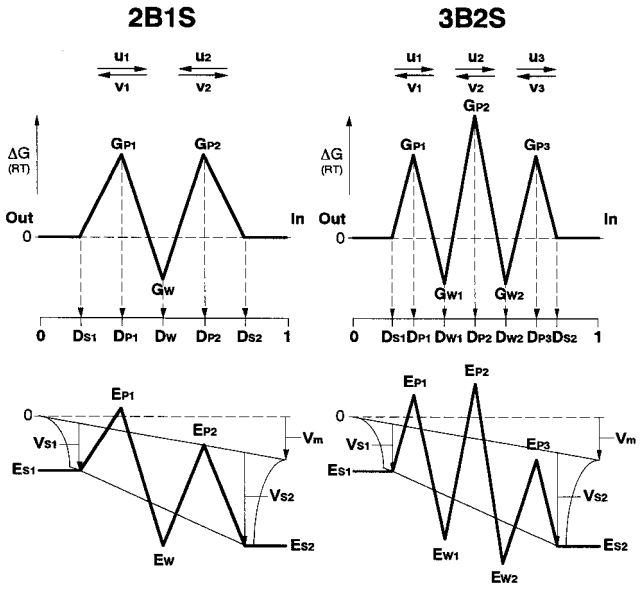

FIGURE A1 Schematic diagrams of the 2B1S and 3B2S pore models describing the kinetics of ion translocation in an open Na-channel. (*Top*) General free energy profiles to define the intrinsic permeability property of the channel pore. The symbol G stands for the Gibbs free energy in RT units at the energy peak (G_P) or well (G_W), and D in the abscissa is the electrical distance from the outside at the pore entrance (D_S), energy peak (D_P), or well (D_W). The reference energy state (*zero level*) corresponds to that of a 1 M salt solution. (*Bottom*) Energy profiles for the channel with negatively charged vestibules at the membrane potential V_m. The electrostatic contribution of the vestibule surface potential V_S and V_m is incorporated into the energy diagrams. The total free energy E at the pore entrance (E_S), energy peak (E_P), or well (E_W) can be expressed as a function of G, D, V_m, and V_S (Eqs. A1–A3). The subscripts 1–3 for G, D, E, and V_S refer to the position with respect to the outside. The symbols u and v at the top represent the rate constants for ion translocation.

where G represents the reduced chemical, and V represents electrostatic energies in RT units, corresponding to the conventional free energy divided by RT and the conventional voltage multiplied by zF/RT, respectively. The cation activities in the outer and inner compartments are denoted a_{ex} and a_{in}, respectively. Assuming the electrochemical equilibrium (Boltzmann distribution) of permeant cations in a channel vestibule and those in a bulk solution adjacent to the vestibule, E_{Si}, is set equal to an electrochemical potential of the permeant cation in the bulk solution. For the 3B2S double-occupancy pore, an ionic repulsion factor was incorporated into the expressions for E_{Pi} and E_{Wi} (see Hille and Schwarz, 1978; Ravindran et al., 1992; Schild and Moczydlowski, 1994).

Rate constants of ion translocation

Rate constants for ion translocation over the energy barriers were formulated in terms of the Eyring's absolute reaction rate theory (Hille, 1975). The rate constant $\mathbf{u}_i$ can be related to the standard Gibbs free energy of activation, i.e., the energy barrier height ΔG, by an exponential function,

$$\mathbf{u}_i = \kappa \cdot (kT/h) \cdot \exp(-\Delta G/RT), \tag{A4}$$

where kT/h is the molecular vibration frequency taken as approximately $5.90 \times 10^{12}\ s^{-1}$ at 10°C, and κ is the transmission coefficient set equal to unity. Thus, the rate constants $\mathbf{u}_i$ and $\mathbf{v}_i$ for the 2B1S pore are given by

$$u_1 = (kT/h) \cdot a_{ex} \cdot \exp(-E_{P1}) \tag{A5}$$

$$u_2 = (kT/h) \cdot a_{in} \cdot \exp(-E_{P2} + V_m) \tag{A6}$$

$$v_1 = (kT/h) \cdot \exp[-(E_{P1} - E_W)] \tag{A7}$$

$$v_2 = (kT/h) \cdot \exp[-(E_{P2} - E_W)], \tag{A8}$$

and those for the 3B2S single-occupancy pore are given by

$$u_1 = (kT/h) \cdot a_{exp} \cdot \exp(-E_{P1}) \tag{A9}$$

$$u_2 = (kT/h) \cdot \exp[-(E_{P2} - E_{W1})] \tag{A10}$$

$$u_3 = (kT/h) \cdot \exp[-(E_{P3} - E_{W2})] \tag{A11}$$

$$v_1 = (kT/h) \cdot \exp[-(E_{P1} - E_{W1})] \tag{A12}$$

$$v_2 = (kT/h) \cdot \exp[-(E_{P2} - E_{W2})] \tag{A13}$$

$$v_3 = (kT/h) \cdot a_{in} \cdot \exp(-E_{P3} + V_m). \tag{A14}$$

For the 3B2S double-occupancy pore, the rate constants for a pore with the inner site occupied (u_1, v_1) or with the outer site occupied (u_3, v_3) were corrected for the repulsion factor A/d_i as an interaction energy between adjacent cations,

$$u_1 = (kT/h) \cdot a_{ex} \cdot \exp(-E_{P1}) \cdot \exp(-A/d_2) \tag{A15}$$

$$v_1 = (kT/h) \cdot \exp[-(E_{P1} - E_{W1})] \cdot \exp(A/d_1 - A/d_2) \tag{A16}$$

$$u_3 = (kT/h) \cdot \exp[-(E_{P3} - E_{W2})] \cdot \exp(A/d_1 - A/d_3) \tag{A17}$$

$$v_3 = (kT/h) \cdot a_{in} \cdot \exp(-E_{P3} + V_m) \cdot \exp(-A/d_3), \tag{A18}$$

where A is the repulsion energy between two monovalent cations at unit electrical distance, and d_i is the electrical distance from an occupied well as defined by $d_1 = D_{W2} - D_{W1}$, $d_2 = D_{W2} - D_{P1}$, and $d_3 = D_{P3} - D_{W1}$.

Mathematical description of dynamic pore model

Mathematical expressions of rate constants

The rate constants for cation binding ($u = u_1 + u_2$) and unbinding ($v = v_1 + v_2$) in a pore of conformation X (u_X, v_X; $X = A, B$) are given by

$$u_X = (kT/h) \cdot \{a_{ex} \cdot \exp(-E_{P1X}) + a_{in} \cdot \exp(-E_{P2X} + V_m)\} \tag{A19}$$

$$v_X = (kT/h) \cdot \{\exp[-(E_{P1X} - E_{WX})] + \exp[-(E_{P2X} - E_{WX})]\} \tag{A20}$$

$$E_{PiX} = G_{PiX} + D_{Pi} \cdot V_m + V_{Pi},$$

$$E_{WiX} = G_{WiX} + D_{Wi} \cdot V_m + V_{Wi} \quad (i = 1, 2).$$

The rate constants for the transition between **A** and **B** (α, β) can also be expressed as exponential functions of the activation energy ΔG,

$$[\alpha, \beta] = [(kT/h) \cdot \exp(-\Delta G_\alpha), (kT/h) \cdot \exp(-\Delta G_\beta)], \tag{A21}$$

where ΔG_α and ΔG_β are the reduced energies (in RT units) of the transition-state with respect to **A** and **B**, respectively.

Calculation of ionic currents

The mathematical procedure for computing steady-state ionic currents (for any concentrations of permeant cations at any V_m) is similar to that previously described for static pore models (e.g., Begenisich and Cahalan,

1980a). The rate equations for the schemes shown in Fig. 7 can be written in a matrix form,

$$dP/dt = K \cdot P. \tag{A22}$$

Here, P and K are the matrices for probabilities of individual states at time t and for transition rate constants, respectively, being given by

$$P = [P_{AO}, P_{AX}, P_{BO}, P_{BX}]', \tag{A23}$$

$$K = \begin{bmatrix} -(u_A + \alpha_O) & v_A & \beta_O & 0 \\ u_A & -(v_A + \alpha_X) & 0 & \beta_X \\ \alpha_O & 0 & -(u_B + \beta_O) & v_B \\ 0 & \alpha_X & u_B & -(v_B + \beta_X) \end{bmatrix}, \tag{A24}$$

where the probability of a pore to be in state X is denoted P_X. In a steady state, each time derivative term is set equal to zero (i.e., $K \cdot P = 0$). Thus, with the conservation equation $\Sigma P_X = 1$, we have

$$D \cdot P = R, \tag{A25}$$

$$D = \begin{bmatrix} -(u_A + \alpha_O) & v_A & \beta_O & 0 \\ u_A & -(v_A + \alpha_X) & 0 & \beta_X \\ \alpha_O & 0 & -(u_B + \beta_O) & v_B \\ 1 & 1 & 1 & 1 \end{bmatrix}, \tag{A26}$$

$$R = [0, 0, 0, 1]'. \tag{A27}$$

Once all the rate constants for the transition matrix D are determined, Eq. A25 can be solved for the matrix P by deriving the inverse matrix D^{-1} (i.e., $P = D^{-1} \cdot R$); and the steady-state probabilities of a pore to be in the allowable states are given by the last column of the matrix D^{-1}. Then, the steady-state net ionic current I flowing through a single Na-channel at a given concentration and V_m can be computed by

$$I = -z \cdot e \cdot [(u_{A1} \cdot P_{AO} - v_{A1} \cdot P_{AX}) + (u_{B1} \cdot P_{BO} - v_{B1} \cdot P_{BX})], \tag{A28}$$

where e stands for the elementary charge.

This work was supported in part by Grant for Project Research from Kanazawa Medical University (P98-6).

REFERENCES

Begenisich, T. B., and M. D. Cahalan. 1980a. Sodium channel permeation in squid axons. I. Reversal potential experiments. *J. Physiol.* 307: 217–242.

Begenisich, T. B., and M. D. Cahalan. 1980b. Sodium channel permeation in squid axons. II. Non-independence and current-voltage relations. *J. Physiol.* 307:243–257.

Bénitah, J.-P., R. Ranjan, T. Yamagishi, M. Janecki, G. F. Tomaselli, and E. Marban. 1997. Molecular motions within the pore of voltage-dependent sodium channels. *Biophys. J.* 73:603–613.

Cahalan, M., and T. Begenisich. 1976. Sodium channel selectivity. Dependence on internal permeant ion concentration. *J. Gen. Physiol.* 68: 111–125.

Cai, M., and P. C. Jordan. 1990. How does vestibule surface charge affect ion conduction and toxin binding in a sodium channel? *Biophys. J.* 57:883–891.

Chandler, W. K., and H. Meves. 1965. Voltage clamp experiments on internally perfused giant axons. *J. Physiol.* 180:788–820.

Chesnoy-Marchais, D. 1985. Kinetic properties and selectivity of calcium-permeable single channels in *Aplysia* neurones. *J. Physiol.* 367: 457–488.

Colatsky, T. J., and R. W. Tsien. 1979. Sodium channels in rabbit cardiac Purkinje fibers. *Nature (Lond.)* 278:265–268.

Correa, A. M., R. Latorre, and F. Bezanilla. 1991. Ion permeation in normal and batrachotoxin-modified Na^+ channels in the squid giant axon. *J. Gen. Physiol.* 97:605–625.

Dani, J. A. 1986. Ion-channel entrances influence permeation. Net charge, size, shape, and binding considerations. *Biophys. J.* 49:607–618.

Dani, J. A., and J. A. Fox. 1991. Examination of subconductance levels arising from a single ion channel. *J. Theor. Biol.* 153:401–423.

Demo, S. D., and G. Yellen. 1992. Ion effects on gating of the Ca^{2+}-activated K^+ channel correlate with occupancy of the pore. *Biophys. J.* 61:639–648.

Doyle, D. D., Y. Guo, S. L. Lustig, J. Satin, R. B. Rogart, and H. A. Fozzard. 1993. Divalent cation competition with [^{3}H]saxitoxin binding to tetrodotoxin-resistant and -sensitive sodium channels. A two-site structural model of ion/toxin interaction. *J. Gen. Physiol.* 101:153–182.

Draber, S., R. Schultze, and U. Hansen. 1991. Patch-clamp studies on the anomalous mole fraction effect of the K^+ channel in cytoplasmic droplets of *Nitella*: an attempt to distinguish between a multi-ion single-file pore and an enzyme kinetic model with lazy state. *J. Membrane Biol.* 123:183–190.

Ebert, G. A., and L. Goldman. 1976. The permeability of the sodium channel in *Myxicola* to the alkali cations. *J. Gen. Physiol.* 68:327–340.

Eisenberg, R. S. 1990. Channels as enzymes. *J. Membrane Biol.* 115:1–12.

Eisenman, G., and R. Horn. 1983. Ionic selectivity revisited: the role of kinetic and equilibrium processes in ion permeation through channels. *J. Membrane Biol.* 76:197–225.

Favre, I., E. Moczydlowski, and L. Schild. 1995. Specificity for block by saxitoxin and divalent cations at a residue which determines sensitivity of sodium channel subtypes to guanidinium toxins. *J. Gen. Physiol.* 106:203–229.

French, R. J., E. Prusak-Sochaczewski, G. W. Zamponi, S. Becker, A. S. Kularatna, and R. Horn. 1996. Interactions between a pore-blocking peptide and the voltage sensor of the sodium channel: an electrostatic approach to channel geometry. *Neuron* 16:407–413.

French, R. J., J. F. Worley, III, W. F. Wonderlin, A. S. Kularatna, and B. K. Krueger. 1994. Ion permeation, divalent ion block, and chemical modification of single sodium channels. Description by single- and double-occupancy rate-theory models. *J. Gen. Physiol.* 103:447–470.

Garber, S. S., and C. Miller. 1987. Single Na^+ channels activated by veratridine and batrachotoxin. *J. Gen. Physiol.* 89:459–480.

Garber, S. S. 1988. Symmetry and asymmetry of permeation through toxin-modified Na^+ channels. *Biophys. J.* 54:767–776.

Gómez-Lagunas, F., and C. M. Armstrong. 1994. The relation between ion permeation and recovery from inactivation of *Shaker* B K^+ channels. *Biophys. J.* 67:1806–1815.

Green, W. N., L. B. Weiss, and O. S. Andersen. 1987. Batrachotoxin-modified sodium channels in planar lipid bilayers. Ion permeation and block. *J. Gen. Physiol.* 89:841–872.

Hainsworth, A. H., R. A. Levis, and R. S. Eisenberg. 1994. Origins of open-channel noise in the large potassium channel of sarcoplasmic reticulum. *J. Gen. Physiol.* 104:857–883.

Hanck, D. A., and M. F. Sheets. 1992a. Time-dependent changes in kinetics of Na^+ current in single canine cardiac Purkinje cells. *Am. J. Physiol.* 262:H1197–H1207.

Hanck, D. A., and M. F. Sheets. 1992b. Extracellular divalent and trivalent cation effects on sodium current kinetics in single canine cardiac Purkinje cells. *J. Physiol.* 454:267–298.

Heinemann, S. H., and F. J. Sigworth. 1990. Open channel noise. V. Fluctuating barriers to ion entry in gramicidine A channels. *Biophys. J.* 57:499–514.

Heinemann, S. H., and F. J. Sigworth. 1991. Open channel noise. VI. Analysis of amplitude histograms to determine rapid kinetic parameters. *Biophys. J.* 60:577–587.

Hille, B. 1972. The permeability of the sodium channel to metal cations in myelinated nerve. *J. Gen. Physiol.* 59:637–658.

Hille, B. 1975. Ionic selectivity, saturation, and block in sodium channels. A four-barrier model. *J. Gen. Physiol.* 66:535–560.

Hille, B., and W. Schwarz. 1978. Potassium channels as multi-ion single-file pores. *J. Gen. Physiol.* 72:409–442.

Horn, R., J. Patlak, and C. F. Stevens. 1981. The effect of tetramethylammonium on single sodium channel currents. *Biophys. J.* 36:321–327.

Huang, L. M., W. A. Catterall, and G. Ehrenstein. 1979. Comparison of ionic selectivity of batrachotoxin-activated channels with different tetrodotoxin dissociation constants. *J. Gen. Physiol.* 73:839–854.

Ikeda, S. R., and S. J. Korn. 1995. Influence of permeating ions on potassium channel block by external tetraethylammonium. *J. Physiol.* 486:267–272.

Khodorov, B. I. 1985. Batrachotoxin as a tool to study voltage-sensitive sodium channels of excitable membranes. *Prog. Biophys. Molec. Biol.* 45:57–148.

Khodorov, B. I., and S. V. Revenko. 1979. Further analysis of the mechanisms of action of batrachotoxin on the membrane of myelinated nerve. *Neuroscience.* 4:1315–1340.

Kimitsuki, T., T. Mitsuiye, and A. Noma. 1990. Negative shift of cardiac Na^+ channel kinetics in cell-attached patch recordings. *Am. J. Physiol.* 258:H247–H254.

Kiss, L., and S. J. Korn. 1998. Modulation of C-type inactivation by K^+ at the potassium channel selectivity filter. *Biophys. J.* 74:1840–1849.

Kurata, Y., I. Hisatome, M. Tsuboi, H. Uenishi, G. Zhang, M. Oyaizu, R. Sato, and S. Imanishi. 1998. Effect of sulfhydryl oxidoreduction on permeability of cardiac tetrodotoxin-insensitive sodium channel. *Life Sci.* 63:1023–1035.

Läuger, P., W. Stephan, and E. Frehland. 1980. Fluctuation of barrier structure in ionic channels. *Biochim. Biophys. Acta.* 602:167–176.

Läuger, P. 1985. Ionic channels with conformational substates. *Biophys. J.* 47:581–591.

Lux, H. D., E. Carbone, and H. Zucker. 1990. Na^+ currents through low-voltage-activated Ca^{2+} channels of chick sensory neurons: block by external Ca^{2+} and Mg^{2+}. *J. Physiol.* 430:159–188.

Makielski, J. C., M. F. Sheets, D. A. Hanck, C. T. January, and H. A. Fozzard. 1987. Sodium current in voltage clamped internally perfused canine cardiac Purkinje cells. *Biophys. J.* 52:1–11.

Matteson, D. R., and R. P. Swenson, Jr. 1986. External monovalent cations that impede the closing of K channels. *J. Gen. Physiol.* 87:795–816.

Mironov, S. L. 1992. Conformational model for ion permeation in membrane channels: a comparison with multi-ion models and applications to calcium channel permeability. *Biophys. J.* 63:485–496.

Mitra, R., and M. Morad. 1985. A uniform enzymatic method for dissociation of myocytes from hearts and stomachs of vertebrates. *Am. J. Physiol.* 249:H1056–H1060.

Moss, G. W. J., and E. Moczydlowski. 1996. Rectifying conductance substates in a large conductance Ca^{2+}-activated K^+ channel: evidence for a fluctuating barrier mechanism. *J. Gen. Physiol.* 107:47–68.

Mozhayeva, G. N., A. P. Naumov, Y. A. Negulyaev, and E. D. Nosyreva. 1977. The permeability of aconitine-modified sodium channels to univalent cations in myelinated nerve. *Biochim. Biophys. Acta.* 466: 461–473.

Naranjo, D., and R. Latorre. 1993. Ion conduction in substates of the batrachotoxin-modified Na^+ channel from toad skeletal muscle. *Biophys. J.* 64:1038–1050.

Neyton, J., and M. Pelleschi. 1991. Multi-ion occupancy alters gating in high-conductance, Ca^{2+}-activated K^+ channels. *J. Gen. Physiol.* 97: 641–665.

Nilius, B. 1988. Calcium block of guinea-pig heart sodium channels with and without modification by the piperazinylindole DPI 201-106. *J. Physiol.* 399:537–558.

O'Leary, M. E., and R. Horn. 1994. Internal block of human heart sodium channels by symmetrical tetra-alkylammoniums. *J. Gen. Physiol.* 104: 507–522.

Oxford, G. S., and J. Z. Yeh. 1985. Interactions of monovalent cations with sodium channels in squid axon. I. Modification of physiological inactivation gate. *J. Gen. Physiol.* 85:583–602.

Pérez-Cornejo, P., and T. Begenisich. 1994. The multi-ion nature of the pore in *Shaker* K^+ channels. *Biophys. J.* 66:1929–1938.

Ravindran, A., H. Kwiecinski, O. Alvarez, G. Eisenman, and E. Moczydlowski. 1992. Modeling ion permeation through batrachotoxin-modified Na^+ channels from rat skeletal muscle with a multi-ion pore. *Biophys. J.* 61:494–508.

Ravindran, A., L. Schild, and E. Moczydlowski. 1991. Divalent cation selectivity for external block of voltage-dependent Na^+ channels prolonged by batrachotoxin. Zn^{2+} induces discrete substates in cardiac Na^+ channels. *J. Gen. Physiol.* 97:89–115.

Richard, E. A., and C. Miller. 1990. Steady-state coupling of ion-channel conformations to a transmembrane ion gradient. *Science.* 247: 1208–1210.

Schild, L., and E. Moczydlowski. 1994. Permeation of Na^+ through open and Zn^{2+}-occupied conductance states of cardiac sodium channels modified by batrachotoxin: exploring ion–ion interactions in a multi-ion channel. *Biophys. J.* 66:654–666.

Schild, L., A. Ravindran, and E. Moczydlowski. 1991. Zn^{2+}-induced subconductance events in cardiac Na^+ channels prolonged by batrachotoxin. Current–voltage behavior and single-channel kinetics. *J. Gen. Physiol.* 97:117–142.

Sheets, M. F., B. E. Scanley, D. A. Hanck, J. C. Makielski, and H. A. Fozzard. 1987. Open sodium channel properties of single canine cardiac Purkinje cells. *Biophys. J.* 52:13–22.

Sheets, M. F., and D. A. Hanck. 1992. Mechanisms of extracellular divalent and trivalent cation block of the sodium current in canine cardiac Purkinje cells. *J. Physiol.* 454:299–320.

Shuba, Y. M., V. I. Teslenko, A. N. Savchenko, and N. H. Pogorelaya. 1991. The effect of permeant ions on single calcium channel activation in mouse neuroblastoma cells: ion-channel interaction. *J. Physiol.* 443: 25–44.

Tsushima, R. G., R. A. Li, and P. H. Backx. 1997a. Altered ionic selectivity of the sodium channel revealed by cysteine mutations within the pore. *J. Gen. Physiol.* 109:463–475.

Tsushima, R. G., R. A. Li, and P. H. Backx. 1997b. P-loop flexibility in Na^+ channel pores revealed by single- and double-cysteine replacements. *J. Gen. Physiol.* 110:59–72.

Visentin, S., A. Zaza, A. Ferroni, C. Tromba, and C. DiFrancesco. 1990. Sodium current block caused by group IIb cations in calf Purkinje fibres and in guinea pig ventricular myocytes. *Pflügers Arch.* 417:213–222.

Wells, G. B., and J. C. Tanaka. 1997. Ion selectivity predictions from a two-site permeation model for the cyclic nucleotide-gated channel of retinal rod cells. *Biophys. J.* 72:127–140.

Yamamoto, D., J. Z. Yeh, and T. Narahashi. 1984. Voltage-dependent calcium block of normal and tetramethrin-modified single sodium channels. *Biophys. J.* 45:337–344.

Yamamoto, D., J. Z. Yeh, and T. Narahashi. 1985. Interactions of permeant cations with sodium channels of squid axon membranes. *Biophys. J.* 48:361–368.